DOI: 10.1002/ ((please add manuscript number))
Article type: Review

Single-Walled Carbon Nanotubes in Emerging Solar Cells: Synthesis and Electrode Applications

*Il Jeon, Rong Xiang, Ahmed Shawky, Yutaka Matsuo, and Shigeo Maruyama**

Dr. I. Jeon, Dr. R. Xiang, Dr. A. Shawky, Prof. Y. Matsuo, Prof. S. Maruyama
Department of Mechanical Engineering, School of Engineering, The University of Tokyo, 7-3-1 Hongo, Bunkyo-ku, Tokyo 113-8565, Japan

Dr. A. Shawky
Nanomaterials and Nanotechnology Department, Advanced Materials Division, Central Metallurgical R&D Institute (CMRDI), P.O. Box 87 Helwan, Cairo 11421, Egypt

Prof. Y. Matsuo
Hefei National Laboratory for Physical Sciences at Microscale, University of Science and Technology of China, 96 Jinzhai Road, Hefei, Anhui 230026, China

Prof. S. Maruyama
Energy NanoEngineering Laboratory, National Institute of Advanced Industrial Science and Technology (AIST), Tsukuba 305-8564, Japan

E-mail: maruyama@photon.t.u-tokyo.ac.jp

Keywords: single-walled carbon nanotubes, carbon electrodes, photovoltaics, organic solar cells, perovskite solar cells

Emerging solar cells, namely organic solar cells and perovskite solar cells, are the thin-film photovoltaics that have light to electricity conversion efficiencies close to that of silicon solar cells while possessing advantages in having additional functionalities, facile-processability, and low fabrication cost. To maximize these advantages, the electrode components must be replaced by materials that are more flexible and cost-effective. Researchers around the globe have been looking for the new electrodes that meet these requirements. Among many candidates, single-walled carbon nanotubes have demonstrated their feasibility as the new alternative to conventional electrodes, such as indium tin oxide and metals. This review discusses various growth methods of single-walled carbon nanotubes and their electrode applications in thin-film photovoltaics.

1. Introduction

Energy is one of the biggest challenges that our society is facing. Global warming and the energy security have prompted society to look for pollution-free and renewable energy sources. Among the different renewable energies available, solar energy is by far the most abundant and cleanest. Photovoltaics, more generally known as solar cells, are semiconducting devices that convert solar energy into electricity, potentially meeting the world's energy demands while avoiding carbon-emissions. Solar cells have received much attention, especially in the last ten years, because of growing concerns over the energy security. Among different types of photovoltaics, silicon solar cells give power conversion efficiencies (PCEs) of over 26% with excellent durability. This technology has already reached the market, and the products are readily available. However as recent technologies, such as flexible smartphones and IoT (internet of things), evolve into more versatile and portable electronics, there is a shift of demand from performance-centric technologies to versatility-oriented technologies. In other words, the paradigm is shifting to flexible, wearable, and light-weight electronic devices. Energy-generating devices are also following the same path. This means that the thin-film solar cell technologies, such as organic solar cells (OSCs)[1–3] and perovskite solar cells (PSCs),[4,5] are considered to be the wave of the future with their critical attributes of being ultra-thin (<1 mm), light-weight, and solution-processable.[6] These emerging thin-film solar cells have the potential to equal or surpass the PCE of silicon solar cells while having major advantages in terms of production cost, enhanced design and a variety of new functionalities. Furthermore, tandem photovoltaics[7], which are combined solar cells of PSCs, silicon solar cells,[8] or OSCs[9,10], are another new and promising category for the future photovoltaic technology. Despite different names of solar cell types, the device structure is largely the same. They commonly share the typical configuration of one photoactive layer in the center, two charge

selective layers above and below the active layer, and two electrodes at each end—at least one of which has to be transparent so that sunlight can pass through it. While there has been an intense efficiency race within the emerging thin-film solar cell community, less attention has been paid to other features, such as flexibility and stability. These traits can be enhanced by using new electrodes and charge-selective layers. Not only the functionalities but also photovoltaic performance is heavily dependent on the electrode and the charge-selective layers. Many scientists around the world, thus far, have focused on these layers by developing novel materials and modifying conventional materials to push the boundaries of current thin-film photovoltaic technology.

Abundant and mechanically resilient carbon allotropes are composed of carbon atoms only, yet manifest different electronic properties depending on their configurations and arrangements. Of the carbon species, carbon nanotubes (CNTs) are promising materials to be incorporated into the thin-film solar cells owing to a wide range of properties ranging from conductors to semiconductors with different bandgaps based on their atomic structure. While the CNTs can have a multiple number of walls, single-walled carbon nanotubes (SWNTs) discovered by Iijima and Ichihashi,[11] can have higher transparency and conductivity[12] than multi-walled carbon nanotubes (MWNTs) because of the difference in their optical transmittance for the same current density. For this reason, SWNTs have already been exploited as electrodes in many electronic devices, replacing both brittle indium tin oxide (ITO) transparent electrodes and expensive metal electrodes.[13–16].

In this review, we discuss selective synthetic growth methodologies of SWNT conductors, and the progress made in the electrode application of SWNTs in the emerging thin-film solar cells. The synthetic growth section is divided into two parts, ‘Classical CVD methods’ and ‘Recent trend in SWNT synthesis’. We review them chronologically to show their history and highlight the progress of the classical preparation methods as well as the new trend. In the second part of the review, we discuss SWNT-electrode applications in the emerging thin-film

solar cells, specifically OSCs and solid-state-sensitized solar cells, with the latter including dye-sensitized solar cells (DSSCs) and PSCs, from their prototypes to the most recent reports. The electrode applications are divided into the transparent electrode application section and top electrode application section. In section 3.3., we discuss thin-film solar cells in which both electrodes are SWNTs. The methodological approaches, problems, and expected benefits differ greatly, depending on the type of electrode being substituted. The scientific details and prospects of the applications are reviewed thoroughly. In the concluding part of this review, the future research outlook on the SWNT-electrode applications in the emerging thin-film solar cells is discussed. Furthermore, areas which deserve further investigation for the advancement of this field are outlined point by point.

2. Synthesis of SWNT Films for Electrode Application

Early studies on the production of SWNTs were centered around arc discharge and laser ablation, in part because SWNTs were discovered as a by-product of an arc discharge process for preparing metal nanoparticles and endohedral fullerenes.[11] However, researchers quickly realized that a more effective method was necessary for the advancement of SWNT research and industrial applications. When chemical vapor deposition (CVD) appeared, it was recognized by the SWNT research community to be a promising method. Among several prototype works conducted in parallel, the two most widely recognized reports were published by Dai *et al*. in 1996,[17] and Kong *et al*. in 1998.[18] After those seminal studies, CVD quickly emerged as the predominant method for SWNT synthesis due to its relatively low cost, high efficient, and scalable nature. Now it has been 20 years, and a great deal of exciting progress has been made with more than thousands of papers in both academia and industry. It would be impossible to cover all of the outstanding work done by the whole SWNT research community. Therefore, we focus on a brief history of CVD synthesis and highlight those, which made a

significant impact on the electrode applications. Because the epicenter of this review is the electrode application in the emerging photovoltaics, the perspective and discussion will be centered around the morphology and properties of the SWNT products. Specifically, we discuss different types of SWNT films produced by different process. Our main goal in this section is to help distinguish the difference between the SWNT film syntheses.[19] During the growth of CNTs using the CVD method, nanoparticle transition metal catalysts play a vital role, because the nanotubes are grown directly on them. Accordingly, we introduce two types of CVD-utilized SWNT film syntheses based on the form of catalysts: One of the methods is introducing the catalysts in a gas-phase, in which both the catalysts and the reactant gas of carbon-containing molecule (hydrocarbon, alcohol, etc.) are fed into a furnace. The other method is using the catalysts embedded on a substrate. In this method, the catalysts are fixed at a certain position and heated under a flow of gas of carbon-containing molecule in a furnace. The former method has an advantage of easy control of the CNT orientation. Thus, the former method is suitable for a large-scale synthesis on account of the nanotubes being free from the catalytic supports. The latter method can be further classified into two based on the shape of their catalyst supports: gas phase growth and supported growth. The schematics showing these two major CVD protocols are presented in **Figure 1a, b and c**. It should be noted that the supported growth can be described as the on-substrate growth when a large and flat wafer is used as a support.

2.1. Classical CVD methods

2.1.1 Gas-Phase Growth

Traditional production methods of SWNTs, such as arc discharge of metal-doped carbon[11] electrodes or laser vaporization of metal-doped carbon targets,[20] were limited to macroscopic scale quantities. Gas-phase CVD, on the other hand, has the potential for a large-scale SWNT production since it is a continuous process involving both catalyst particle formation and SWNT nucleation.[21] Direct product collection in the absence of support material

reduces the amount of processing steps and costs. Many groups have investigated gas-phase continuous flow production of thick MWNTs (called Endo fiber). These studies typically involve passing a mixture of carbon source gas and organometallic catalyst precursors through a heated furnace. The organometallics decompose and react, forming clusters on which MWNTs nucleate and grow. Endo and colleagues carried out studies on the production of MWNTs by this method, using mixtures of molecules such as ferrocene and hydrocarbons. However, the operating conditions and growth mechanism of the SWNT production process were substantially different from those of the MWNTs production, resulting in a much smaller tube diameter with only a single graphene shell.

The earliest gas-phase production method was the high-pressure carbon monoxide (HiPco) process, which was developed at Rice University by Smalley and collegues (**Table 1: Process A**).[22] HiPco was the first process that allowed the production of gram-scale quantities of SWNTs, and triggered an explosion of studies on various properties of SWNTs. Large-scale production (>10 g/day) of high-purity SWNTs is possible through this method.[23] Even today, many research groups utilize the HiPco process to produce starting materials for various SWNT applications. Also, HiPco SWNTs are most thoroughly studied SWNTs by optical methods due to their high-quality and suitable diameter range. What is more, the HiPco process can be said to be the forebear of the other SWNT production processes, for its remarkable influence on the subsequently developed methodologies of not only for the electrode applications but also for the purely semiconducting SWNT productions. For this method, an Fe-containing organic precursor, $Fe(CO)_5$, is introduced into the hot zone of a furnace and decomposed to form nano-sized Fe particles under high-pressure (10-30 atm) and high-temperature (900–1100 °C).[23] Heating decomposes $Fe(CO)_5$ into $Fe(CO)_n$, where n = (0–4), produces Fe atoms condensed into clusters. The clusters then serve as catalytic nuclei upon which the SWNTs nucleate and grow in the gas phase via CO disproportionation (the Boudouard reaction): $CO + CO \Rightarrow CO_2$ + SWNTs. The raw HiPco product contains a high weight percentage of catalyst particles. After

a purification process, the metal impurity can be reduced to <0.1%.[22] Another significant aspect of the HiPco process is a use of the oxygen-containing molecule, CO, as a carbon source. This brought a major impact for the developments of other CVD methods that came later, for example, CoMoCAT, which also uses CO as a carbon source (**Table 1: Process B**),[25] and alcohol catalytic CVD (ACCVD), which uses ethanol (**Table 1: Process C**).[26-27] Ethanol later became one of the most popular carbon sources for the laboratory-scale production of SWNTs. An obvious drawback of the HiPco process is the harsh growth requirements of a high temperature and 10-30 atm of a CO flow. Therefore, efforts were made to develop a new process that has milder growth conditions. A few years later, H. M. Cheng et al. proposed an approach, in which instead of using $Fe(CO)_5$ and CO, ferrocene as the Fe catalyst precursor and benzene as the carbon source were employed. This was one of the earliest gas-phase production methods which allowed a growth in an atmospheric pressure (**Table 1: Process D**).[28] These modifications resulted in long rope-like strands containing mostly SWNTs. As no high-pressure system is used, the reactor is much simpler compared with the HiPco process. Using this method, the same group recently obtained isolated SWNT networks for a conductive transparent film application (**Figure 2a-c**).[29,30] The film is highly conductive, having a record low sheet resistance of 41 ohm $sq.^{-1}$ with 90% transmittance at 550 nm of wavelength (**Figure 2d**). After acid doping, the sheet resistance further decreased to 25 ohm $sq.^{-1}$, which is close to that of ITO. Such superior performance is attributed to two important characteristics of the produced film. First, the length of the SWNTs is long (tens to hundreds of micrometer) and the SWNT network has less bundles (85% tubes isolated). Second, the SWNTs are linked by graphitic carbons, which made the junctions of metallic and semiconducting SWNTs near-ohmic contacts.

Further progress was reported by introducing thiophene as a promoter for the SWNT production. The role of sulphur in thiophene in the SWNT synthesis is still not fully understood even today, but sulphur is widely used as an additive for the CVD production of SWNTs, such as enhanced direct injection pyrolytic synthesis (eDIPS) (**Table 1: Process E**).[31] The eDIPS

process was first proposed about 10 years ago at AIST by Saito and collegues[32], and has since been domestically scaled up. eDIPS is classified as the gas-phase growth, but a toluene solution of nanoparticle catalysts is injected into a vertical reactor through a spray nozzle. In this process, the concentration (solubility) of the catalyst is crucial for high-yield, but too much high concentration can lead to aggregation of the nanoparticles. So, the development of catalysts, which has excellent solubility in organic solvents, is important for a successful large-scale production using the eDIPS method. eDIPS traditionally uses catalysts that are derived from an Fe-containing compound (ferrocene), but a more efficient growth can be achieved by using different hydrocarbons as the carbon source from ethylene to various aromatic liquids.[33] Different carbon sources also results in producing SWNTs with different ranges of diameter and chirality.[34] Due to a high temperature used in eDIPs, even mass-produced eDIPS SWNTs have high crystallinity. Their G/D ratio, which is the intensity of the "graphitic" G-band over the intensity of the "disorder" D-band, as measured by Raman spectroscopy, exceeds 100; the higher value indicates higher crystallinity of SWNTs. SWNTs prepared by eDIPS are commercially available. The examples of gas-phase CVDs described above usually produce SWNTs as fluffy powder, long ropes, or bulky aggregates.

One of the major breakthroughs in the electrode applications of SWNTs is the floating-catalyst aerosol SWNT synthesis, which produces free-standing and uniform thin films collected directly on a filter paper (**Table 1: Process F**).[35] In this process, CO or ethanol are used as a carbon source, and CO_2 are sometimes introduced as an additional gas.[36,37] The film obtained by filtering the gas phase contains very long, high-quality SWNTs in a random network with high uniformity (**Figure 2e**). Films prepared in this method are highly flexible and have an ITO-comparable sheet resistance (< 80 Ω $sq.^{-1}$ with 90% transparency). Therefore, these films are perfect for the electrode applications. By controlling the bundling of SWNTs in the gas phase, isolated SWNT-dominant networks can even be obtained.[38-39] Due to the small bundle size and narrow diameter distribution of these SWNTs, now the films can be produced

in diverse colors (**Figure 2f**). These colored SWNT films are obtained by a CO_2-assisted CVD, in which the concentration of CO_2 is to tuned to control the chirality and diameter range of the products (**Figure 2g-i**).[40] These colors are originated from the sharp absorption of SWNTs with a narrow diameter distribution and the absence of bundle- or impurity-induced background absorption. The electrode applications of these SWNT films in the emerging thin-film photovoltaics have already been demonstrated by many groups. Thus far, this type of SWNT-electrodes has been found to be the most promising for the photovoltaic electrode applications for both transparent and non-transparent, especially for the flexible application.

2.1.2 Supported Growth

In contrast to the previous growth techniques where the formed catalysts are floating in a gas phase, the supported growth utilizes active catalyst particles that are fixed on a supporting material. The supporting materials are usually porous oxides with nano-spaces and large surface areas. The nano-spaces hold the catalyst particles and are spacious enough for the SWNT growth which requires few nanometers of space in general. The large specific surface area provides more nucleation sites for more efficient growth. Zeolite is one of the good examples of these catalyst supports (**Table 1: Process G**).[41] The necessity of regular zeolite pores and the correlation between the pore size and nanotube diameter, however, are still under debate, There are also reports on a successful growth by silica, alumina (Al_2O_3), MgO, and other metal oxide nano-power.[42] These materials are directly implanted onto the supporting materials. However, in both zeolite and oxide nano-powder's cases, a specific catalyst loader is needed, which differentiates this approach from the gas-phase growths discussed above.

One of the successfully established supported growth techniques is the CoMoCAT process[25] developed by Resassco and colleagues (**Table 1: Process B**). This process is readily used in preparing commercially available SWNTs and the starting materials used in many research. As can be deduced from its name, this process uses a novel binary catalyst: Co-Mo.

This combination was a classical model catalyst for efficient growths of SWNTs, and prompted further studies exploring other binary catalyst combinations. One of the distinct features of CoMoCAT SWNTs is their small diameter. Photoluminescence excitation-emission mapping indicates that CoMoCAT SWNTs are (6,5)-enriched, though we do recognize that the photoluminescence has a limited detection range and cannot detect metallic tubes. In this system, Mo is believed to stabilize Co and keeps it from aggregating into larger particles. This understanding and mechanism have also influenced many later studies.

The discovery of ACCVD by Maruyama et al. was also the important contributions made to the CVD synthesis of SWNTs (**Table 1: Process C**).[26] Unlike CO and methane, which are toxic and requires a high temperature, respectively, alcohol is an environmentally friendly and cheap carbon source; in the case of CoMoCAT process, CO is used as a carbon source and magnesia is used as a catalyst support. Another unique advantage of ACCVD is that a use of alcohol allows much milder reaction condition, particularly a low growth temperature down to 550°C. A more recent report has shown the operating window which can be lowered even further down to 400°C.[43] ACCVD-produced SWNTs are usually clean and free of amorphous carbon, which is attributed to the etching effect by oxygen atom in ethanol. Ethanol has quickly become one of the most popular carbon sources for the laboratory-scale production of SWNTs. The first vertically aligned SWNT array was also produced by ACCVD.[44] Due to the wide operating window of the ACCVD process, the range of SWNT diameter and chirality can be widely modulated.[45] For example, (5,4) tubes with ultra-small diameters can be produced by this method.[43] The ACCVD process, despite having the advantages of low temperature and clean growth, has yet to be commercialized due to some limitations, specifically requirement of a low working-pressure.

In the on-substrate growth, the catalysts are loaded onto a flat wafer. This leads to a unique feature of the on-substrate growth, which is that the SWNTs can be aligned horizontally

or vertically on a substrate. However, application of the on-substrate growth of SWNTs is rarely reported in solar cells because of the limited production quantity of SWNTs owing to the limited surface area of the flat substrates. Yet, the on-substrate growth is the most representative system for many fundamental studies, such as those who endeavor to understand the properties and growth principles of SWNTs.

Here we briefly review the history and highlight recent breakthrough in the growth of semiconducting arrays. When the catalyst is loaded onto a flat wafer at a high density, SWNTs support each other and lift off the substrate due to the crowding effect, resulting in a high-density forest-like SWNT array standing on the substrate. This phenomenon was first discovered by Murakami *et al*. in the name of ACCVD2 process (**Table 1: Process H**).[44] The key importance to growing a vertically aligned SWNT (VA-SWNTs) array is ensuring that the catalysts are small, dense, and efficient (**Figure 1e**). The small size is to retain growth selectivity; the high density is to form an array; and the high efficiency is important for growing SWNTs long enough to form a macroscopic array. As a follow-up of this work, "super-growth" process, in which enhanced growth efficiency was achieved by incorporating a trace amount of water into ethylene CVD (**Table 1: Process I**), was reported.[46] This super-growth process was later demonstrated in many proof-of-concept applications, and recently been used in mass production by Zeon Co. Inc.[47] In a VA-SWNT array, the catalyst particles sit on the substrate and stay only at the substrate-SWNT interface. The array itself is, therefore, pure. The top of an array is usually a crust of tangled SWNTs, which help the SWNTs grow simultaneously at the same rate. Consequently, the SWNTs have a similar length, and the entire film is highly uniform. Thanks to these geometric advantages, many elegant studies have been conducted using this system, including demonstration of growth kinetics by *ex* or *in situ* monitoring[48,49] and anisotropic optical/electronic properties,[50,51] manipulation/patterning of the CNT films,[52–54]

modulation of the SWNT structure,[55–57] and fabrication of a high-efficiency filter.[58] There is even a VA-SWNT electrode application in Si solar cells.[59]

The other alignment that can be achieved on a substrate is a parallel growth. One of the earliest examples is a gas-oriented growth, which usually produces sparse but long SWNTs parallel to the substrate (**Table 1: Process J**).[60-63] In this type of growth, tubes fly along the gas flow, and the catalyst are located at the tips of the SWNTs. The mechanism of this growth is the well-accepted "kite" model.[61] The catalyst can remain active for many hours and produce half-meter CNTs[64] or CNT bundles with a tensile strength over 80 GPa.[65] The history and recent progress is well summarized in a good review paper.[66] Crystal lattice-assisted growth is a favored strategy for practical growth of horizontally aligned SWNTs (HA-SWNTs) (**Table 1: Process K**) (**Figure 1f**). In this method, the atomic arrangement of the surface rather than the gas flow, unlike the previous example, guides the growth of SWNTs.[67-69] The most effective substrates were sapphire and single-crystal quartz. High efficiency with good alignment can be achieved on many cuttings and facets with little influence from the gas flow. This method produces pure SWNTs because MWNTs are too thick to be aligned with the lattice and cannot grow out of the catalysts. Also, the density of SWNTs can be much higher than the previously mentioned flow-guided methods. Much progress has been achieved in the development of this process for demonstrations of selective growth or removal,[70] high-density growth, [71] and etc. High-density HA-SWNT arrays are believed to be the most promising SWNT material for electronics and even the first CNT computer was demonstrated using this type of SWNTs.[72] However, many fundamental issues remain to be addressed. In particular, the purity of semiconducting tubes is still not satisfactorily high, even though tremendous efforts have been made to date. Further, the SWNTs in the array having diverse lengths and wafer non-uniformity is another issue to be resolved. One of the recent progress in this method is the work by the Jiang and collegues at Tsinghua University. They succeeded in growing 99.9% pure semiconducting SWNT arrays by switching the electric field *in situ* during the CVD synthesis

(**Figure 3**).[73] The concept behind this work is that extra electrons in the region of catalyst particles modulate the re-nucleation barrier, which leads to a highly-selective renucleation of semiconducting SWNTs. (**Figure 3a**) In this work, they used SEM contrasts to identify metallic SWNTs from their semiconducting conterparts,[74-76] which is a highly convenient and reliable technique developed by the same group for imaging horizontal SWNT arrays (**Figure 3b**). Using this technique, the junctions between the metallic and semiconducting SWNTs are clearly visualized (**Figure 3c**). The authors predict that the metallic impurity may be further reduced down to 1 ppm when the average diameter of SWNTs is tuned to 1.3 nm. In addition, since the produced SWNTs are almost defect-free, an FET fabricated on hundreds of SWNTs shows a high ON/OFF ratio together with a high ON current. This breakthrough, if extendable to other growth conditions, is expected to accelerate the development of SWNT-based electronic devices.

Overall, SWNT films outperform MWNTs as an electrode despite low dispersibility. Thus far, randomly oriented SWNTs produced by gas-phase growth has been the most promising for the electrode applications. We are continuing to improve the conductivity and transparency of this SWNT films from the synthesis level. On the same note, we are in search of HA- and VA-SWNT electrode applications as well.

2.2. Recent trend in SWNT synthesis

2.2.1. Chirality Selective Growth from Solid Catalyst

Chirality-controlled production is considered the Holy Grail in the SWNT community that right synthesis conditions have been sought after over decades.[77] However, characterization and quantification of the chirality population of an as-grown sample are challenging, let alone understanding the mechanism that governs SWNT chirality. Early attempts were mostly based on photoluminescence, which does not visualize all SWNTs. One breakthrough was reported by Li and colleagues, who proposed a novel catalyst using the

combination of Co and W.[78] This Co-W combination forms an intermetallic Co_7W_6 compound, which is solid at a high temperature. These solid catalysts follow a vapor-solid-solid model and selectively produce (12,6) SWNTs from the (0,0,12) facet. In this work, they used Raman spectroscopy to check all SWNTs one-by-one and obtained statistical data that were difficult to achieve before. Together with the absorption spectroscopy, atomic force microscopy, electron diffraction, the Raman results provide strong evidence for the high selectivity, which exceeds 95%. The mechanism was interpreted based on DFT calculations, which revealed a facet-dependent energy match. Using this strategy, (14,4)-, (16,0)- and (18,7)-enriched SWNTs could be prepared.[79,80] The selectivity of the Co-W catalyst was confirmed in the follow-up study, where Co-W catalysts were prepared by a different method and an intermediate structure of Co_6W_6C was identified.[81] In contrast to the previous strategy in which catalyst structure and facet determined the chirality, Zhang and colleagues proposed that both catalyst symmetry and the SWNT growth kinetics are important. They used rather unique Mo_2C and WC catalysts to produce (12,6) and (8,4) SWNTs with a selectivity of 80%. Since the catalysts were prepared on a sapphire substrate, the obtained SWNTs were horizontally aligned. Such well aligned, high-density, (2m,m)-selective growth is expected to advance the electrode applications of SWNTs in electronics.[82]

There are also reports on the selective growth of other chiralities of SWNTs, particularly near the armchair, though the mechanism is not well understood. For example, Chen and colleagues obtained (9,8)-enriched SWNTs from a supported catalyst. [83,84] They emphasize the importance of sulfur in the Co/SiO_2 catalyst. To incorporate S into catalyst preparation, they started from $CoSO_4$ precursor and confirmed that the use of a sulfate-promoted catalyst is the key. [85] In this process, calcination of the catalyst is found to be critical for the SWNT selectivity, as the catalyst is converted into different Co species at different pre-treatment temperatures. [86] Another example is the successful synthesis of (6,4) nanotube, which was previously produced in a much lower abundance than other nanotubes with similar diameters, e.g. (6,5). [87] In this

report, the authors tuned the oxidation degree of Co and found a small difference in the oxidation degree resulting in a drastic change from (6,5) to (6,4) nanotubes.

2.2.2. High yield SWNT cloning

Cloning is an ideal concept for producing single-chirality SWNTs. However, research in this direction has been progressing slowly because of the two main challenges: the low efficiency in cloning growth and the unavailability of single-chirality seeds. In recent year, great progress has been made on both of these challenges, making cloning more practical for a structure-controlled growth of SWNTs.

One of the main contributors to this research direction is Zhang and colleagues at Peking University. They showed the first experimental evidence that a SWNT can extend its length without changing their chirality. The extended part duplicated the structure of the parent SWNT (or called seeds), so this process is named to be SWNT cloning (**Figure 5a**).[88] In this process, no additional catalyst is involved and carbon precursors are directly added to the open-ends of an SWNT. The growth rate is, therefore, very slow. Furthermore, since SWNT extends only at the activated edge, the cloning success ratio is not high: only a few percentages of SWNTs can extend its original length from the original recipe. A recent report by the same group proposed a microwave-assisted CVD method, in which the damaged parts of the original SWNTs can be regenarated and SWNTs can curl themselves at moderate CVD conditions.[89] With the assistance of a microwave, the activation ratio can reach 100%. This method is expected to achieve a high yield SWNT cloning.

The second challenge is that SWNT cloning should be achieved from single-chirality, pre-defined SWNT seeds. This was demonstrated by Zhou and colleagues. They employed the chirality-pure SWNTs from DNA-assisted separation, and confirmed that the cloning growth of (7,6), (6,5) and (7,7) nanotubes can be achieved (**Figure 5b**). [90] This is the first demonstration of SWNT cloning from a pre-defined, and solution processed SWNTs, which

opened up the possibility of combining two different approaches: a solution-based chirality sorting and vapor-based CVD growth. Using a similar approach, they also studied the growth dynamics of various SWNTs with different chiralities, and clearly evidenced that the growth rate of a near armchair nanotube like (6,5) is higher than a near zigzag (10,1) nanotube. [91] The lifetime of these two tubes are, however, found to be opposite.

Lastly, we emphasize another different approach of growing structure defined SWNTs from molecular rings. This research direction is pioneered by Itami and colleagues at Nagoya University. Their scenario can be interpreted as an extreme condition of SWNT cloning, where the starting seeds do not exist but only organic-chemistry-synthesized molecular rings (cycloparaphenylenes) do.[92,93] This is an excellent strategy for controlling the structure of the SWNTs, because the starting molecules can be designed according to the target chirality. In their proposal, armchair SWNTs may be produced with diameter ranges from 1.2 nm to 2.2 nm using available cycloparaphenylenes molecules. The key issue here is the stability of the ring molecules. In a more recent synthesis, they successfully solved this long-lasting problem and obtained a carbon nanobelt, which is a closed loop of fully fused edge-sharing benzene rings (**Figure 5c**). [94] This molecule is expected to produce (6,6) nanotubes. However, there is a significant gap in the operation condition between organic molecule synthesis and SWNT CVD production.

While these long-awaited breakthroughs are encouraging and attracting great attention, controlled production techniques are still far from perfect. For example, only a few types of chirality can be selectively produced. The mechanism for chirality selectivity and the origin of SWNT chirality in CVD are also under debate.[95] Efficient and reliable characterization on structures of catalyst is still not easy. [96] However, there is room for further improvement of yield and growth uniformity. We still need more patience before chirality, property, structure-controlled SWNT films appear and play a key role in electronics including the thin-film solar cell.[97]

3. SWNT-electrode Applications in Emerging Thin-film Solar Cells

3.1. Problems of Conventional Electrode

A vital feature common to photovoltaics is their transparent conductor through which light travels before reaching the photo-active layer. Conventionally, ITO or fluorine-doped tin oxide (FTO) have been used as the transparent electrode because of their exceptionally high conductivity and transmittance unparalleled by any other materials. However, there have been many attempts to replace these metal oxide transparent conductors due to their high cost arising from limited abundance.[98] In addition to this, the brittleness of the metal oxides is said to be the sole limiting factor for the flexible application of solar cells.[99] Therefore, the alternative transparent electrode has to be not only highly conductive and transparent but also mechanically resilient, cost effective, and easy to fabricate.[100–104] In this regard, SWNTs are considered to be a good candidate for a transparent conductor, because SWNTs have good optical transparency over a broad range of wavelengths along with high electrical conductivity.[41,105–107] Moreover, the SWNT-electrodes have much higher mechanical resilience than ITO, while possessing an advantageous work function of around −5.0 eV, which is similar to that of ITO. The potential raw cost of SWNT fabrication is also lower than that of ITO, owing to the abundance of carbon on the earth's surface. Metal electrodes, which are normally used as the top charge collector, also have problems. Although they do not hinder the flexible applications because of their ductile nature, they are expensive and tedious to deposit for their high melting point. Costly thermal deposition has to be used via a shadow mask method, which leads to a waste of materials. Even though there are solution-processable metal electrodes, such as silver paste, their conductivity is lower than that of thermally deposited metal electrodes, and the

material cost is still high. In addition to the fabrication cost, metal electrodes lower the stability of PSCs, which will be discussed in detail in a later section.

3.2. SWNT-electrodes in Organic Solar Cells

As environmental and energy conservation problems have surfaced globally, thin-film solar cells have attracted great interest among the researchers. Of the different types of solar cells, silicon solar cells are dominant in the current photovoltaic market, owing to their high PCE and stability. Nevertheless, the weight, rigidity, and high cost of silicon are still a barrier to a mass production at an industrial level. OSCs, however, can obviate the shortcomings of silicon solar cells because they possess low-cost processability and flexible applicability, as well as the potential to exhibit PCEs as high as those of silicon solar cells. Subsequent to the Nobel prize-winning discovery of conductive polymers,[108] solution-processed bulk-heterojunction organic photovoltaics were reported in 1995.[109] Three to four years later, starting around 1999, there was an inundation of publications on bulk-heterojunction OSCs and a dramatic increase in the reported PCEs of the solar devices. The rate of increment was around 65% every year.[110] The reason for such an explosion of OSCs was the tantalizing prospect that OSCs might supersede silicon solar cells on account of their superior qualities of light weight, flexibility, and printability.[111–113] Initially, OSCs harnessed conductive organic compounds, such as polymeric electron donors and fullerene-based electron acceptors. In addition to the lack of batch-to-batch reproducibility of the polymers, both fullerene derivatives and polymers have limited stability in air. Both species become oxidized in air and aggregation can undo the bulk-heterojunction mix over time; moreover, fullerenes dimerize and decompose to different compounds. Furthermore, their limited light absorption range and limited charge mobility constrain the photovoltaic efficiency. Owing to these problems, the maximum PCEs of traditional OSCs could not exceed 11%, which is considerably lower than the PCEs of

conventional silicon solar cells—about 25%. Nevertheless, in recent years, there have been breakthroughs in OSCs with the discovery of stable low-bandgap polymers[114,115] and non-fullerene acceptors[116,117]. Now the PCE exceeds 13% with higher stability ascribed to the fact that the bulk-heterojunction mixture is retained as a result of the non-aggregative nature of non-fullerene acceptors and their intrinsic stability. CNT electrode application has been following the trend of OSC development. Introduction of new materials to OSC systems means that the compatibility between CNTs and the new materials should be tested.

3.2.1. SWNT as Transparent Electrode

The first report of SWNTs replacing the ITO electrode in OSCs was published by Chhowalla and colleagues at Rutgers in 2005.[118] The SWNT-electrode-based OSCs produced a PCE of 0.99%, which was higher than that of the ITO-based control devices; they ascribe the excellent performance to the three-dimensional nature of the interface between the SWNTs and the poly(3-hexylthiophene):phenyl-C61-butyric acid methyl ester (P3HT:PCBM) nanocomposite (**Table 2: Device A, Figure 6a**). This work is particularly significant as the SWNT-electrode was solution-processed as opposed to the vacuum-deposition of ITO. They controlled the SWNT volume which had a direct influence on the surface resistivity of the films. Grüner and colleagues at UCLA further improved a similar device architecture by using much more transparent and highly conductive SWNTs via a transfer printing method, involving dimethylpolysiloxane (PDMS),[119] and employing a more optimized photo-active layer thickness.[120] Their OSC devices were fabricated on PET substrates for flexible demonstration. These flexible SWNT-based OSCs produced a much higher PCE of 2.5% while possessing excellent mechanical flexibility (**Table 2: Device B, Figure 6b**). They also controlled the SWNT film resistivity by tuning the amount of SWNTs. Subsequently, Chhowalla and colleagues reported flexible SWNT-based OSCs using filtration-transferred SWNT films as a cathode rather than as an anode.[121] The device was an inverted-type architecture where ZnO

nanowires are grown on SWNTs. In general, it is difficult to deposit metal oxides on carbon electrodes because of different surface wettability. They used the ZnO nanowire growth method, which allows the coating of ZnO on carbon electrodes. A PCE of 0.6% was recorded with no record of accurate photovoltaic parameters but a *J*–*V* curve (**Table 2: Device C, Figure 6c**). The fact that the series resistance (R_S) and shunt resistance (R_{SH}) seem to be low from the *J*–*V* curve, which indicates that the low efficiency was caused because that the ZnO nanowires had little or no doping effect on the SWNTs. In addition, the energy levels might not have aligned well.[16] Franghiadakis and colleagues[122] reported on a spin-coated SWNT-electrodes in OSCs which has a similar structure to the devices reported by Grüner and colleagues[120] (**Table 2: Device D, Figure 6d**). Although their exhibited PCE of 1.2% was lower than 2.5% PCE produced from the flexible devices reported by Grüner and colleagues, who used spin-coated SWNT-electrodes which has a substantial merit for its low-cost processability and large-size applicability. They used HiPco-synthesized SWNT solution stabilized by the surfactant, sodium dodecylsulfate (SDS) to disperse in a solvent. Moreover, they used poly(3,4-ethylenedioxythiophene) polystyrene sulfonate (PEDOT:PSS) alone as an electrode without SWNTs, but the performance was not high. However, this approach became the seed for the future work involving PEDOT:PSS electrodes (**Table 2: Device E, Figure 6d**).[123] Another fascinating aspect of this work[122] is that the solution-processed SWNT films are submerged in ethanol (EtOH) for the removal of the SDS. This improved the conductivity of the film substantially. Kim *et al.* also reported solution-processed SWNT-electrode-based OSCs in 2010.[124] They reported a PCE of 2.3% owing mainly to the use of LiF before Al deposition and HNO_3 doping. They compared the use of different surfactants for the SWNT solution: They tested a SWNT solution free of surfactants in dichloroethane, aqueous SWNTs with added SDS, and aqueous SWNTs with added sodium dodecylbenzenesulfonate (SDBS). The SWNT solution with no surfactant and the OSCs that had been spray-processed with the SDS-added SWNT produced PCEs of 2.3% and 2.2%, respectively, which were comparable to the 2.3% of

the ITO-based OSCs (**Table 2: Device F and G**). It is worth noting that the spin-coated SWNTs without surfactant produced higher PCEs, but the spray-coated surfactant added-SWNT-electrodes showed higher conductivity. They spin-coated EtOH on top of the SWNT-electrodes to improve the wettability during the fabrication, but there was no attempt to remove the surfactants. Hersam and colleagues[125] reported ITO-free OSCs utilizing SWNT-electrodes with varying metallic tube compositions sorted by density gradient ultracentrifugation (**Table 2: Device H, Figure 6e**).[126] To minimize the roughness of SWNT films, they employed dip-coating of SWNT aqueous solutions containing 2% w/v Triton X-100 [$C_{14}H_{22}O(C_2H_4O)_n$; n=10], followed by soaking in HNO_3 to remove residues. Such process was time-consuming but offered a high degree of control over the film thickness and roughness. It was fascinating and enlightening that they focused on different CNT compositions, and CNTs with 100% metallic SWNTs were indeed the best for the electrodes in OSCs. This was followed by the work of Salvatierra *et al.*, who used thin films of polyaniline/CNT nanocomposites as a transparent electrode in fluorene-thiophene polymer (F8T2)-based OSCs (**Table 2: Device I, Figure 6f and 6g**).[127] Polyaniline is reported to be more conductive and chemically stable than PEDOT:PSS.[128,129] This work is noteworthy because they used a new solution-processed method to produce transparent CNT electrodes, and a new organic photo-active layer was employed. Thus, it is worth mentioning in this review, even though the CNTs that they used were not SWNTs, but multi-walled CNTs.[130] A great leap in PCE occurred when Jeon *et al.* used a low-bandgap polymer system on MoO_x-doped SWNTs (**Table 2: Device J**, **Figure 7a**).[131] Poly({4,8-bis[(2-ethylhexyl)oxy]benzo[1,2-b:4,5-b']dithiophene-2,6-diyl}{3-fluoro-2-[(2-ethylhexyl)carbonyl]thieno[3,4-b]thiophenediyl}) simply known as PTB7 and phenyl-C71-butyric acid methyl ester ($PC_{71}BM$) were used as electron donors and acceptors, respectively in OSCs. Using low-bandgap polymers, such as PTB7, results in high photovoltaic performance on account of the longer wavelength absorption that leads to a high J_{SC}, and higher mobility which translates to a high fill factor (FF).[132] PTB7 has a low-lying highly-occupied

molecular orbital (HOMO) which induces a high V_{OC}. The PTB7-based OSC devices produced a PCE of 7.31% when ITO was used as the electrode. MoO_3-and-PEDOT:PSS-deposited SWNT-electrode-based OSCs produced a PCE of 5.3%. Thermal annealing the MoO_3 next to the CNTs in an anaerobic condition was reported by Bao and colleagues[133] of Stanford University to produce effective and stable doping. MoO_3 turned into MoO_x after the doping with x being between 2 and 3. Trap sites were created by heating MoO_3 to a high temperature, and the electrons in the CNTs hopped onto the MoO_x. The same approached was used in this work and MoO_x-doped SWNT-OSCs exhibited a PCE of 6.0%, which was the record-high efficiency among the SWNT-transparent-electrode-based OSCs in 2015 (**Table 2: Device K**). Beside the record high efficiency, the significance of this work comes from the analysis of SWNT-electrodes with different transparency. SWNT films which 65% of 550 nm wavelength light is being transmitted (subsequently referred to as T65% SWNT), T80% SWNT, and T90% SWNT were compared in OSCs. The higher the transparency of the SWNT-electrodes, the lower conductivity of the SWNT-electrodes was. As SWNT-electrodes with both the maximum transparency and conductivity are desired in OSCs, it was discovered that the T65% SWNT-electrode performed better for the PTB7-system devices, due to the intrinsic high absorption of longer wavelengths. In addition, flexible applications were demonstrated using the two types of plastic substrates, polyimide (PI) and polyethylene terephthalate (PET). PI has a glass transition temperature greater than 200 °C, which is higher than that of PET. As MoO_x doping requires high-temperature annealing, PI was tested, in spite of the fact that PI has a lower transmittance than PET. PI-based flexible SWNT OSCs produced a PCE of 3.4%, which—surprisingly—was lower than that of PET-based flexible SWNT OSCs in which MoO_3 was not annealed (**Table 2: Device L and M**). There was a clear difference in J_{SC} arising from the lower transparency of PI; however, the FF was surprisingly similar in both types of devices. A cyclic flexural test showed that the PET-based flexible OSCs was much more mechanically robust than the PI-based flexible OSCs (**Figure 6b**). Maruyama and colleagues of The University of

Tokyo demonstrated the same OSCs with SWNTs electrodes using small molecule diketopyrrolopyrrole (DPP(TBFu)$_2$) (**Table 2: Device N, Figure 6c**).[103] It was the first small-molecules OSCs using SWNT-electrodes. The small molecules have attracted many OSC researchers owing to their high absorption coefficient, fast charge transport, and enhanced miscibility with the fullerene acceptors.[134,135] In addition, they have lower batch-to-batch variation and are easier to modify than their polymer counterparts. However, the performance was not as high as the low-bandgap polymer case. The high open-circuit voltage (V_{OC}) and FF were high, but the short-circuit current density (J_{SC}) was substantially low. According to the analyses conducted, it was found that the morphology of the small molecule-based bulk heterojunction layer was remarkably poor when spin-coated on SWNT-electrodes. We surmised that the small molecules might have seeped into the CNT network and this led to the separation of the small molecule donors from the fullerene acceptors.

3.2.2. SWNT as Top Electrode

CNT or any other carbon electrode material has rarely been reported for use as top electrodes in place of metals in OSCs, on account of the difficulty in laminating carbon electrodes and doping them. Because of the chemical and physical sensitivity of the organic active layer, the application is extremely difficult. For instance, soft organic active layers can be damaged during the lamination of CNT. Moreover, it is a general practice that we apply solvents to improve the interface between the top CNT electrode and the layer underneath. However, in the case of OSCs, casting non-polar solvents on top of CNT electrodes will damage the active layer. Further, applying polar solvents will damage the hole-transporting layers as well as crumple the CNT electrode, which is hydrophobic. Considering these facts, Matsuo and colleagues at The University of Tokyo came up with a novel methodology of SWNT top electrode application and their doping.[136] A normal type architecture with ZnO electron-transporting layers and MoO_3 hole-transporting layers was used. Metal electrodes were replaced

by SWNT films to produce metal-free OSCs for window applications (**Figure 8a**). **Figure 8b** shows the different types of OSCs fabricated in this work. In order to achieve doping without damaging other layers underneath, two novel fabrication methodologies were invented (**Figure 8c and 8d**). The HNO_3 doping sandwich-transfer method uses another glass substrate on which an HNO_3-doped SWNT-electrode is pre-laminated. The pressing force of the top electrode substrate improves the interface between the carbon electrode and the underlying layer, giving a PCE of 4.1% for the T60%-SWNT (**Table 2: Device O**) and 3.7% for the T90%-SWNT (**Figure 8c**). The MoO_x doping bridge-transfer method is slightly more burdensome in terms of its fabrication. It requires a specially designed shadow mask for the deposition of MoO_3 on SWNT. This procedure was necessary to anneal the entire MoO_3-deposited SWNT film mounted on a holder (**Figure 8d**). In this way, thermal damage to the OSC system could be avoided during the thermal annealing of SWNTs. However, the PCE was not as high as that of the devices produced by the HNO_3 doping sandwich-transfer method. We ascribe the low efficiency to the poor contact between the SWNT-electrode and the active layer. There are two possibilities: One is that there is no external force applied to press the SWNT-electrode, and another is that some portion of the SWNT film is crumpled while it hangs precariously over the holder during the fabrication process.

3.3. SWNT-electrodes in Solid-State-Sensitized Solar Cells

3.3.1. Dye-Sensitized Solar Cells

DSSCs, also known as ‘Grätzel cell’ is based on a semiconductor formed between a photo-sensitized anode and an electrolyte. It was originally co-invented by Grätzel and O'Regan at UC Berkeley in 1988 and later published with a descent PCE of approximately 7.9% in 1991.[137] It was sensational at the time invention as it involved low-cost materials during a simple fabrication, which allowed the use of conventional roll-printing techniques. The

invention of DSSC served a critical role in the field of emerging thin-film solar cells. It can be said that DSSCs are the harbinger and an inspiration for PSCs, and indeed most of DSSCs researchers now have moved to the PSC research. Analogous to other solar devices, DSSCs have two electrodes in which one of them is called 'counter electrode/working electrode' and the other is called 'transparent electrode'.[138,139] There have been many attempts to replace those electrodes by CNTs. In this section, we briefly go over those reports in a chronological order.

SWNT as Counter Electrode or Transparent Electrode

Expensive Fluorine-doped tin oxide (FTO) substrates coated with a catalytic amount of platinum have been used as counter electrodes in DSSCs, because of their high electrochemical activity. In this case, a low-cost electrode with high electrochemical activity is required to boost the practical utility of DSSCs. Titanium dioxide nanoparticles are widely used as the working electrode in DSSCs because they provide higher efficiency and more robustness than any other metal oxide semiconductor investigated.[140] Occasionally carbon has been used as a catalyst of the counter electrode, because the overvoltage of the iodide/tri-iodide reduction at the carbon catalyst is kept low; see, for example the work by Kay *et al.*, who applied carbon films to the counter electrode of a DSSC and obtained a reasonable PCE (**Figure 9a**).[141] Yanagida and colleagues applied SWNTs (purchased from Carbon Nanotechnologies Inc.) and nano-horns as the counter electrode in DSSCs with a liquid electrolyte[142] to the best of our knowledge, this was the first time this had been attempted (**Figure 9b**). They expected that the favorable contact between nano-fibrous SWNTs and the electrolyte should produce high PCE by enhancing the electrochemical activity of the electrode. Indeed, they obtained a PCE of 4.5%, which is comparable to that of the platinum-sputtered FTO-based standard DSSC devices. This was followed another study by Jang *et*

al.,[143] who investigated the effects of applying acid-treated SWNTs to TiO_2 in DSSCs. Dye-functionalized SWNTs with the acid treatment at the TiO_2/electrolyte interface had a significant effect on photocurrent-voltage characteristics. The DSSCs that used acid-treated and dye-functionalized SWNTs achieved a 25% increase in J_{SC}, which indicates the improved contact between the acid-treated SWNTs and the TiO_2 particles by enhanced light scattering of TiO_2 clusters. The V_{OC} also increased by around 0.1 V. This is due mainly to the basicity of the TiO_2 interface having NH groups of ethylenediamine moieties of the anchored dyes on SWNTs. Kamat and colleagues reported SWNTs in DSSCs as both electrodes and charge transporters.[144] The SWNTs functioned as conducting scaffolds in DSSCs to produce a PCE of 0.2%, which is twice as high as the 0.09% PCE of the devices without SWNTs. TiO_2 was scattered onto the SWNT film, improving photo-induced charge separation and transport of carriers to the electrode. Achieving the charge equilibrium between TiO_2 and SWNTs was paramount for the solar cell performance. In 2010, Li *et al.* reported novel titanium nitride (TiN)-CNT counter electrode-based DSSCs which produced a PCE of 5.41%.[145] The TiN-CNT electrodes were prepared by thermal hydrolysis of $TiOSO_4$ on CNTs and subsequent nitridation in an ammonia atmosphere. TiN nanoparticles in the 5–10 nm range were dispersed on the surface of the CNTs. TiN demonstrated high electrocatalytic activity for the reduction of tri-iodide ions, because the electronic structure of the metal nitrides is analogous to that of the noble metals. The identity of CNTs was not described in the reported communication, but we surmise it was a mixture of single- and multi-walled CNTs from the provided transmission electron microscope (TEM) images. In the same year, Ouyang and colleagues published a work involving coating gel binder-free films of CNTs in which SWNT and MWNT films were used in DSSC devices. The CNT films were dispersed in low-molecular-weight poly(ethylene glycol) (PEG) through mechanical grinding, ultrasonication, and subsequent removal of PEG by heating. SWNT counter electrodes-based DSSCs showed high PCE and higher stability compared with the Pt counter electrode-based control devices.

A CNT-PEDOT core-shell counter electrode in a DSSC was reported by Im and colleagues.[146] A stable CNT-PEDOT counter electrode was synthesized by chemical oxidative polymerization of 3,4-ethylenedioxythiophene (EDOT) using $FeCl_3$ and dodecylbenzene sulfonic acid (DBSA) as the oxidant and surfactant, respectively (**Figure 9c**). Whereas control devices using CNTs only and PEDOT as the counter electrode produced PCEs of *ca.* 3.88% and 4.32%, respectively, the DSSCs using a CNT-PEDOT core-shell counter electrode gave a PCE of approximately 4.62%, owing to the improvement in FF, that arose from the increased electrical conductivity of the CNT/PEDOT composite. This can be attributed to the doping effect of slightly acidic PEDOT on CNTs. The vertically-aligned CNT forests described by Hill and colleagues can be used as counter electrodes for tri-iodide reduction in DSSCs.[147] They used FTO as the growth substrate. Fluorine was leached from FTO at high temperatures by the process gases, reducing tin oxide to tin metal islands on native oxide. Vertically-aligned CNT forests grown on such substrates were used in DSSCs and produced a PCE of 5.2%, which is lower than the 6.6% of the platinum counter electrode-based DSSCs. Despite the higher V_{OC}, lower J_{SC} and FF led to the lower PCE. The lower J_{SC} and FF came from the lower catalytic effect and high resistance of the vertically-aligned CNT forests, respectively.

SWNT as Both Electrodes

Sun and colleagues reported using SWNTs as both electrodes in DSSCs in 2012.[148] They used ultrathin titanium-sub-oxide to modify SWNT conductive films and harnessed them as the transparent electrode in DSSCs. In addition, for the counter electrode, they used a bilayer of SWNTs and carbon black. The PCE of the DSSCs with both electrodes fabricated from SWNTs depended heavily on the added amount of carbon black and the modification of the ultra-thin titanium sub-oxide. There was an acceleration of electron transfer kinetics at the counter electrode by the carbon black and an inhibition of mass recombination at the

transparent electrode/electrolyte interface by the ultra-thin titanium-sub-oxide, respectively. The best PCE obtained was 1.37%.

3.3.2. Lead Organohalide Perovskite Solar Cells

Since the first demonstrations of the prototype PSC by Miyasaka and colleagues,[149] organic–inorganic halide PSCs have attracted a great deal of attention of the researchers around the globe, because of their ability to soar up the PCE through the heated efficiency race.[5] The real competition began when Park and colleagues[150] and Snaith and colleagues[151] reported novel methods of All-Solid-State Submicron TiO_2 filled with 2,2',7,7'-tetrakis-(N,N-di-4-methoxyphenylamino)-9,9'-spirobifluorene (spiro-MeOTAD) and mesoporous alumina, respectively to boost the PCE of PSCs in 2012. After 6 years of continuous leaps in fundamental insights and fabrication know-hows, PSCs have become one of the emerging thin-film photovoltaics with its best certified efficiency of 23.3% as of today. Now the production at an industrial level is being discussed based on its high PCE, yet there are number of imminent problems to address before commercialization. The prospect of their flexible application and commercialization depends on the flexibility of the used materials, fabrication cost, and stability of the devices. According to literatures,[99,152] the conventional transparent electrode ITO is the sole layer that limits the flexible application as they cause crack under severe bending cycle. Also, the price of ITO is constantly rising and takes up a huge portion in a PSC fabrication. [98] Therefore, the replacement of ITO is crucial to both flexibility application and commercialization of PSCs. This is the same situation as OSCs, but the stark difference can be found in the metal electrode. The stability of PSCs is closed linked to ion migration and moisture barrier-ability of the top electrode, which is different from OSCs.[153] Conventional metal electrodes have problems of oxidation, ion migration, and poor barrier-ability, let alone the expensive material cost and deposition cost.[154–156] This led the researchers to focus on the replacement of the metal electrode in PSCs more than the replacement of ITO. The fact that the

perovskite layer does not dissolve in non-polar solvents made the metal electrode replacement by CNT films easier than that in OSCs. Hydrophobic CNTs can be densified using non-polar solvents, which do not damage the perovskite layer, yet totally destroys organic photoactive layer in the case of OSCs.

This section provides an overview of the application of SWNTs as electrodes in PSCs, replacing ITO and metal in one or both of the electrodes. We start with the case of 'SWNT as Top Electrode' because much research has been done on this approach.

SWNT as Top Electrode

The first demonstration of SWNTs as the top electrode in PSCs was reported by Mhaisalkar and colleagues.[157] They fabricated n-i-p mesostructured perovskite solar cells and laminated aerosol-synthesized SWNT films on top. They discovered that the SWNT film can function as both a hole-transporter and as an electrode. While the mechanism was not specified in the article, the improvement of a relatively low PCE of 6.3% to 9.9% upon the addition of spiro-MeOTAD implies that the charge selectivity of the aerosol-synthesized SWNT films, which are a mixture of semiconducting and metallic SWNTs, was not enough to replace the hole-transporting materials (**Table 3: Device A and B, Figure 10a**). Also, they tested the device performance when the light is shone from the ITO side and SWNT side. The performance was better when the light was shone from the ITO side, on account of higher transparency of ITO over SWNTs. When a separate reflector was introduced on the SWNT side, the PCE increased marginally, revealing that there is a non-reflective limitation to the SWNT top electrode yet it is not significant. In their conclusion, the authors mention that the low conductivity of the SWNT films is one of the limiting factors and that the photovoltaic performance can be enhanced using dopants on the SWNTs. This is regarded to be challenging even to this day, because the SWNT film is laminated on top of various layers and any attempt to dope it can damage the underlying layers.[136] One year later, Wang *et al*., reported a flexible

solar cell in which TiO_2 nanotube arrays were grown on a $TiCl_4$-treated Ti foil electrode and capped by $MAPbI_3$. This was followed by the aerosol-synthesized CNTs (SWNT+DWNT) densified using a spiro-MeOTAD solution (**Table 3: Device C and D, Figure 10b**).[158] Owing to the thin metal foil substrate, the fabricated solar devices were flexible and could retain their efficiency even after 100 bending cycles. While the PSCs without $TiCl_4$ treatment showed a PCE of 4.83% (**Table 3: Device C**), $TiCl_4$ treatment increased the V_{OC} by approximately 200 mV, producing a substantially higher PCE of 7.38% (**Table 3: Device D**). This approach was particularly original because of the way that the researchers harnessed the Ti component for both the conductor and as an electron-transporting layer.[104] PCEs were generally low, this can be ascribed to the fact that light could only be shone from the CNT sides. As discussed before,[157] a relatively low transmittance of CNT limits performance of solar devices. A more advanced follow-up to the work of Mhaisalkar and colleagues was conducted by Aitola *et al.,* using mixed formamidinium lead iodide-methylammonium lead bromide, $(FAPbI_3)_{0.85}(MAPbBr_3)_{0.15}$.[159] Mixed formamidinium lead iodide-methylammonium lead bromide PSCs have been reported to produce higher efficiency and stability than methylammonium lead triiodide perovskite $MAPbI_3$, because of the large bandgap and more compact cubic perovskites.[160] Again, in this work[159], the SWNT film alone could not function fully as a hole-transporter. PSCs without spiro-MeOTAD produced a PCE of 11.0% (**Table 3: Device E**). The photovoltaic performance increased to 15.5% when spiro-MeOTAD was added to the SWNTs. Interestingly, however, J_{SC} did not increase; only V_{OC} and FF increased when the spiro-MeOTAD solution was added (**Table 3: Device F**). They confirmed that spiro-MeOTAD does not have any doping effect on SWNTs and it is solely the aerosol-synthesized SWNTs that have the charge-selective function. Considering that the gold electrode-based control PSCs gave a PCE of 18.8%, the PCE of 15.5% by using the mixed cation perovskite and multi-laminated SWNTs is high but could be improved even further (**Figure 10c**). The investigation was continued in the same architecture, but this time they employed cesium-added

mixed formamidinium lead iodide-methylammonium lead bromide, $Cs_5(MA_{0.17}FA_{0.83})_{95}Pb(I_{0.83}Br_{0.17})_3$ to produce an even higher PCE of 16.6% (**Table 3: Device G**).[161] Moreover, they investigated the thermal stability of the devices by subjecting them to an elevated temperature of 60 °C, which is a commonly used temperature for stability testing of photovoltaics.[162] They measured the continuous time-evolution of the *J–V* curves and the *J–V* metrics over the course of the aging and found that the SWNT-based devices possessed superior long-term thermal stability compared with the gold electrode-based control PSCs (**Figure 10d**). A notable difference came from the substantial reduction in V_{OC} of the control devices which was attributed to the gold ion-migration-induced degradation of the perovskite layer.[162] Kim and colleagues reported PSCs in which CNT paste was applied using the doctor blade method. The CNT paste was purchased from Carbon Nano-Material Technology Co., Ltd. and was mostly multi-walled CNTs. They achieved 10.7% efficiency without the use of spiro-MeOTAD, and the two-step fabrication method was used to embed the perovskite into the network of CNTs (**Table 3: Device H**).[163] Jang and colleagues reported paintable carbon electrode-based perovskite solar cells using CNT dripping.[164] Again, multi-walled CNTs and the perovskite layer were entangled together. Without using spiro-MeOTAD, they achieved the best PCE of 13.6% (**Table 3: Device F**). The CNT-based PSCs lasted much longer than spiro-MeOTAD- and gold-based control devices during the stability test. Thus far, all of the aforementioned SWNT-based PSCs have replied on a TiO_2 electron-transporting layer and spiro-MeOTAD as the hole-transporting material. TiO_2 is responsible for severe hysteresis, owing to trapped charges between the metal oxide and the perovskite interface, which directly impacts the degradation of the perovskite solar cells, undermining the device stability.[165] Spiro-MeOTAD is well known to be thermally unstable, especially at temperatures above 80 °C, which might be the reason why the stability test by Aittola *et al.*,[161] was conducted at 60 °C and their SWNT-based PSCs showed excellent stability over a long period of time.[166–168] In order to maximize the stability potential of the SWNT-based PSCs, Choi and colleagues

developed a novel PSC structure, in which a fullerene layer was used as the electron-transporting layer while a nanocomposite of SWNT and P3HT was used as the electron-blocking top electrode (**Figure 11a**).[169] The device structure was coined 'carbon-sandwiched PSC'. It was discovered (through a combination of simulation and experiment) that the lower chemical capacitance of the fullerene compared with TiO_2 contributes to the reduced hysteresis and longer-lasting durability of the perovskite layer. In addition to this, adding polymeric hole-transporting layers, such as P3HT and poly(triarylamine) (PTAA), to SWNTs instead of spiro-MeOTAD resulted in a much better stability, because the polymer/SWNT combination functioned as a more effective moisture barrier and also had better thermal stability. Even though employing spiro-MeOTAD in the carbon-sandwiched PSCs produced a PCE of 17.0%, the devices did not last as long as the polymer-mixed carbon-sandwiched devices according to the stability test result (**Table 3: Device H**). The reason that PTAA- and P3HT-mixed devices exhibited superior barrier properties—and thus better stability—is that the longer chains of polymers can wrap around SWNTs, thereby effectively sealing the SWNT film. Furthermore, the conjugated polymers induced π–π interactions with the SWNTs, forming supramolecular nanohybrids.[170] Unlike the staggered conformations of PTAA, P3HT has a planar conformation. This allows P3HT to have stacked crystallizations, leading to a more closely packed structure. This is why the P3HT-added PSCs showed a much higher stability than the PTAA-based devices, although the PCE performance was lower for the P3HT-based PSCs. The polymer-containing devices produced moderate PCEs of 15.3% for PTAA (**Table 3: Device I**) and 13.6% for P3HT (**Table 3: Device J**), respectively. However, their stability and low-cost advantages are far greater than in the devices that employed spiro-MeOTAD. In particular, the P3HT-based carbon-sandwiched PSCs were so much stable that the encapsulated devices maintained their PCE more than 2000 hours under operating conditions without a UV filter in ambient light (**Figure 11b**). Having witnessed the potential of SWNT-laminated PSCs, we have collaborated with Yang and colleagues at UCLA by incorporating a new type of perovskite and

the top-SWNT doping through collaboration with the The limitations of SWNT-laminated PSCs lie in the SWNTs not being reflective, and SWNTs having lower conductivity than metals. Therefore, for SWNTs, it was essential to come up with PSCs in which the perovskite photo-active layer can absorb maximum light before it reaches the top SWNT, and to increase the conductivity of SWNTs via a suitable doping method. As a solution to this, we incorporated a formamidinium perovskite layer as the active layer to maximize the light absorption and trifluoromethanesulfonic acid (TFMS) vapor doping to dope the SWNT-electrode without damaging the neighboring layers (**Figure 12a**).[171] Compared with the previously mentioned mixed cations, $Cs_5(MA_{0.17}FA_{0.83})_{95}Pb(I_{0.83}Br_{0.17})_3$, $(FAPbI_3)_{0.85}(MAPbBr_3)_{0.15}$, and $MAPbI_3$; purely FA-based perovskite, $FAPbI_3$ has a small bandgap (E_g) of approximately 1.4 eV, which is the ideal bandgap for the Schockley-Queisser model (**Figure 12b**).[172] This means that $FAPbI_3$ has the highest J_{SC} at the expense of V_{OC} among other types of perovskite layers, and thus can absorb the maximum amount of sunlight extending to a wavelength of 850 nm. However, because of its intrinsic instability, the pure $FAPbI_3$ perovskite is difficult to realize. Yang and colleagues at UCLA developed a technology in which a small amount of 2D perovskite addition surrounds the 3D $FAPbI_3$ perovskite grains, protecting them from moisture.[173] Here, application of this 2D/3D $FACsPbI_3$ architecture enabled the successful fabrication of PSCs based on CNT top electrodes; these PSCs featured very high values of J_{SC}, as well as achieving the vapor doping of TFMS.[174] A mild vapor doping of SWNT top electrode allowed a fine control of the energy level alignment between the valence level of $FAPbI_3$ and the SWNTs, which led to the increase in V_{OC} (**Figure 12c**). Thirty seconds of vapor-doping time was the optimal time for the overall device performance, because longer vapor doping for more than 30 s resulted in an acid-base reaction between TFMS and the 4-tert-butylpyridine (*t*-BP) in the spiro-MeOTAD solution (**Figure 12d**). In addition to this, a new electron-transporting layer, SnO_2 was employed in SWNT top-electrode-based PSCs for the first time; the more widely used TiO_2, as mentioned, has a problem of severe hysteresis due to

index mismatch and high chemical capacitance. Moreover, TiO_2 triggers trapped-charge-induced degradation of the perovskite layer.[165,175,176] Although replacing TiO_2 by C_{60} greatly improved stability by removing hysteresis, fullerene is still vulnerable to oxidation and will be oxidized by oxygen in the air at some point.[169] SnO_2 has been reported to produce less hysteresis than TiO_2, and because it is more stable than C_{60}, it will not undergo as much oxidation in air.[177,178] Combining all of those factors in one device, a PCE of 17.6% was achieved, which is a record high among the carbon-electrode-based PSCs (**Table 3: Device K, Figure 12e**).

SWNT as Transparent Bottom Electrode

The SWNT film can not only be used as the top electrode but also as the transparent electrode as demonstrated in the OSC section 3.2. The very first replacement of the conventional metal oxide transparent conductor by a carbon electrode in PSCs was demonstrated by Matsuo and colleagues.[179] Inspired by the MoO_x doping of SWNT transparent electrode in OSCs (**Table 2: Device L**),[133] the same approach was used to dope SWNT transparent electrode in PSCs.[179] MoO_x doping which worked in the case of OSCs did not work in PSCs because of the fact that MoO_3 was not energetically compatible with the perovskite layer. There was an energy level alignment mismatch between MoO_3 and $MAPbI_3$.[180,181] The incompatibility of MoO_3 was investigated using an impedance study, and different approaches were proposed to effectively dope the SWNT transparent electrodes in PSCs. To avoid MoO_3, three different methods of doping were showcased: One of the three methods was to apply HNO_3, which is a very effective—yet short-lived—dopant, before spin-coating PEDOT:PSS on top. The second method was to modify PEDOT:PSS by adding 0.5 wt% of a polyoxyethylene(6) tridecyl ether (Sigma Aldrich Chemical Co., Inc.) surfactant to make the solution hydrophobic. Because the SWNT-electrode is intrinsically hydrophobic

without any treatment, it is imperative to control the wettability of the PEDOT:PSS solution to achieve a uniform coating. The last method was to dilute the PEDOT:PSS solution with isopropyl alcohol (IPA) to modify the wettability of the solution, similar to the second method. In the case of HNO_3 doping, various concentrations of HNO_3 were tested. As HNO_3 is difficult to handle, corrosive, and toxic, it is important to know if diluted HNO_3 has the same doping effectiveness. HNO_3 diluted in water by different volume percentages was used to dope SWNTs, and PSCs were fabricated using the doped carbon electrode. The result showed that HNO_3 retained the same doping effectiveness down to 35 v/v% according to the four-probe measurement, vis-NIR spectroscopy, Raman spectroscopy, and photovoltaic performance (**Figure 13a**). In particular, the precise *p*-type doping effect can be quantified by analyzing the upshifted G and 2D Raman spectroscopy bands arising from the phonon stiffening effect, and quenching of the van Hove singularities (E^M_{11}, E^S_{22}, E^S_{11}). All the data pointed to the doping effect of HNO_3 remaining unchanged down to the 35 v/v% dilution. Accordingly, the highest PCE of 6.32% was obtained from 35 v/v% HNO_3-doped SWNT transparent electrode-based PSC (**Table 3: Device L, Figure 13b**). Given that the ITO-based PSCs gave a PCE of around 9%, achieving a 6.32% efficiency from indium-free PSCs was quite an encouraging result at that time. When the surfactant-added PEDOT:PSS was used on the SWNT-electrode directly, a low PCE of 2.71% was obtained (**Table 3: Device M**). This was due to the fact that the perovskite film coating did not give a high-quality film. We attribute the problem to the surfactant-added PEDOT:PSS-soaked SWNT-electrode exhibiting low surface energy, which shortened the anti-solvent dropping time-window. The photovoltaic efficiency was much better for the PSCs to which IPA-diluted PEDOT:PSS had been applied; although their performance was not as high as that of the HNO_3-treated devices, 4.27% was obtained without utilizing dopants (**Table 3: Device N**). In fact, the acidic nature of PEDOT:PSS functioned as a mild dopant and contributed to lowering the sheet resistance. Finally, flexible PSCs were fabricated on PET substrates using HNO_3 as a dopant, giving a PCE of 5.38% (**Table 3: Device O, Figure**

13c). Although the performance of the flexible PSC dropped to 4.60% after enduring a severe cyclic flex test, the efficiency was high enough to generate a reasonable amount of electrical power. Apart from the efficiency, the letter[179] discussed a possible impediment due to an energy level mismatch between the valence band of $MAPbI_3$ and the Fermi level of HNO_3-doped SWNT (**Figure 13d**). It was observed that the series resistance (R_S) of the PSCs was abnormally high when strongly *p*-doped SWNT-electrodes were used. A detailed analysis using impedance spectroscopy showed that irrespective of the intrinsic sheet resistance (R_{Sheet}), SWNT-electrodes with a Fermi level lower than -6.0 eV manifested high resistance when the holes move from perovskite to the electrode. Nearly a year later, Choi and colleagues reported PSCs using transparent graphene electrodes and claimed that MoO_3 is, in fact, compatible with $MAPbI_3$ if an ultra-thin (2 nm or less) layer of MoO_3 is used.[182] They demonstrated an extremely high PCE of 17% from graphene-based ITO-free PSCs, and there was no dopant used during the fabrication. The comparison involving single-layered graphene and SWNTs was conducted by Jeon *et al*.[183] The devices were compared and contrasted in terms of photovoltaic performance and mechanical properties (**Figure 14a**). For the photovoltaic performance, single-layered graphene-based PSCs produced a higher efficiency of 14.2% compared with 12.8% for the SWNT-based PSCs. This was when the ITO-based control devices were typically producing a PCE of 17.8% (**Table 3: Device P and Q**). The overall device efficiencies reported in this work were lower than in the previous report because we had increased the size of the active area and the fabrication was performed during a humid summer season. The main reason for the higher PCE of the graphene-based PSCs was J_{SC}. The graphene-based PSCs produced a J_{SC} of 21.2 mA cm^{-2} whereas the SWNT-based PSCs produced J_{SC} of 17.5 mA cm^{-2}. The main reason for the higher J_{SC} was the higher optical transparency of the single-layered graphene. Its transmittance from the UV-vis spectroscopy was even higher than that of ITO (**Figure 14b**). The V_{OC} was the same because the Fermi levels of the single-layered graphene and SWNT were very similar according to the photoelectron yield spectroscopy (PYS). In the case of the FF, the

SWNT-based PSCs showed a higher FF than the single-layered graphene-based PSCs. We attributed this to the higher R_{Sheet} of the SWNT-electrode compared to the single-layered graphene electrode. As opposed to tenuously connected single-layered graphene, SWNTs are known to have a low number of defect sites, which leads to higher conductivity. In terms of morphology, the SWNT-electrodes displayed much rougher surfaces than the single-layered graphene in the atomic force microscopy (AFM) topographic images. To test the mechanical resilience of the carbon-electrode-based PSCs, a four-probe measurement and Raman spectroscopy were conducted before and after a stretching and bending test. The four-probe measurement shows that after a 200-cycle flexural test, the R_{Sheet} of the single-layered graphene electrode increased by approximately 150 Ω, but only a marginal change was recorded from the SWNT-electrode.[184–186] This was due to the defect formation at the grain boundaries of the graphene films, which the SWNT films did not possess. G band and D band shifts of Raman spectroscopy can visualize how the stretching affects the carbon electrodes. The shift of these peaks with strain is an intrinsic property of hexagonal carbon rings that can be defined by the Grüneisen parameters. The Grüneisen parameters describe how changing the volume of a crystal lattice affects the vibrational Raman frequency of the phonons within the lattice.[187,188] The second-order two-phonon process responsible for the 2D band is caused by the scattering of two iTO phonons near the K point. This mode is independent of defects but dependent on strain.[189] There were stronger shifts of the G and 2D bands in the single-layered graphene electrodes than in the SWNT-electrodes when they were stretched and bent. This indicates that graphene is more susceptible to stress and strain than SWNTs when the same magnitude of the tensile or flexural force is applied. This makes sense as the SWNT films have an entangled geometry of nanotubes, which requires more stretching before the hexagonal carbon rings can be distorted in shape. However, single-layered graphene has a totally flat geometry that allows immediate warping of the original benzene rings when stretched. The difference was more clearly manifested when the SWNT films and the graphene films were used as the transparent

conductors in PSCs and underwent a severe cyclic flexural test. By the time the number of bending cycles reached *ca.* 700, the PCE of the single-layered graphene-based PSCs started to drop before that of the SWNT-based PSCs (**Figure 14c**). It was concluded that the single-layered graphene electrode has the upper hand when it comes to photovoltaic performance. Whereas, the SWNT-electrode has advantages in terms of mechanical resilience, reproducibility owing to easy transfer, and ease of processing. With the result being a tie, when one determines a preference between these carbon electrodes, it should be based on which aspects of solar cells one values more.

SWNT as Both Electrodes

Analogous to OSCs, both electrodes can be made up of carbon electrodes within the same system. We demonstrated PSCs in which SWNT-electrodes functioned as both anode and cathode in an inverted device structure.[190] Initially, we thought that the advantage of using SWNT for both electrodes would lie in its facile and low-cost processability. Unlike the thermal evaporation of metal electrodes and sputtering of ITO, SWNT can easily be laminated. This means that the right structural configuration can be contrived, it is possible to maximize the potential of SWNT-electrode. There are a number of important advantages to using the SWNT-electrodes: The fact that they are laminated means that PSC fabrication can be roll-to-roll (R2R)-processed. The R2R-process is extremely important from an industrial perspective as the process can shorten the Takt-time (the average time between the start of production of one unit and the start of production of the next unit, when these production starts are set to match the rate of customer demand.).[191] The R2R process can also save material costs, and enable large-size device production. Moreover, the carbon materials are cheap and abundantly available as opposed to the metals used for the conventional electrodes. Therefore, we chose

the inverted-type architecture for this study because of its low-temperature processability and solution processability for this study. To obtain a high efficiency in the inverted PSCs, rather complicated multiple layers of electron-transporting materials were necessary: for example, a configuration of ITO/PEDOT:PSS/$MAPbI_3$/C_{60}/bathocuproine(BCP)/LiF/Al. Such stacking gave a PCE of 17.0%, but the materials used were expensive, and thermal evaporation steps in vacuum were unavoidable. However, any process involving a vacuum chamber increases the fabrication cost drastically.[192] PSCs are often presented as a low-cost, solution-processable technology that enables flexible solar cells, but the reality is that if the fabrication process involves a vacuum chamber, then it becomes a high-cost process with no advantage for flexible substrates (**Figure 15a**). Using vacuum chambers in an industrial line means that the fabrication process must be frequently interrupted while a large volume is pumped down to high-vacuum levels; moreover, the installation costs are very high. In addition, the process has to rollback which increases the processing time and causes damage due to bending, static electricity, and physical contact with the substrates of other layers.[193] One of the merits of flexible technology is R2R processability of the plastic substrates; however, involving a vacuum chamber means that the process has to be a sheet-to-sheet (S2S) process, rather than a R2R process if we want to achieve a low-cost process. Consequently, we postulated that a simplified vacuum-free structure would be more suitable for the PSCs with both electrodes based on SWNTs—even at the expense of the PCE loss. The simplified PSCs with a configuration of ITO/PEDOT:PSS/$MAPbI_3$/PCBM/Al produced a PCE of 12.8%. As most of the previously reported carbon electrodes have been anodes, this work emphasizes the importance of SWNT cathode demonstrations. Carbon conductors in air are slightly *p*-doped. Stable and effective *n*-dopants for carbon electrodes have not been reported to the best of our knowledge.[194–196] This makes SWNT cathodes difficult and unattractive. However, in order to achieve PSCs with electrode based on SWNTs, it is paramount that high-performance PSCs in which the SWNTs function as a cathode is realized. When a very thick SWNT cathode (transmittance of 50% at

550 nm wavelength) was laminated from the top and densified using a PCBM solution, a high PCE of 10.5% was obtained. It was found that the application of the PCBM solution decreased R_{Sheet} as measured by the four-probe; and the Raman G and D bands shifted to the left, which may serve as an indication of an *n*-doping effect. When HNO_3-doped highly transparent SWNT films were used as the anode, a PCE of 9.8% was produced (**Table 3: Device R**). This is a remarkable improvement from the previous report in which a PCE of 6.32% was obtained (**Table 3: Device L**). This is ascribed to the adoption of a new PSC fabrication technique, called the adduct method.[197] Having confirmed that the SWNT films can function either as anodes or as cathodes in PSCs, the two systems merged into one. Various device configurations were tested and the most optimized structure was found to be SWNT-P3HT/PEDOT:PSS/$MAPbI_3$/SWNT-PCBM, in which 50% transparent SWNT films were used as the anode and PCBM-mixed 90% transparent SWNT films were used as the cathode. The sunlight was incident on the cathode side. P3HT was necessary for the solar cell to function; we conjecture that this is due to the energy band alignment. Both-SWNT-electrode PSCs produced a PCE of 7.32% and the device structure could potentially be non-stop R2R processable (**Table 3: Device T, Figure 15b**). Moreover, the cost analysis showed that the PSCs with both electrodes composed of SWNTs cost only 57.6% of the conventional PSCs, and when considering industrial-scale scale production, this figure went down even further to 32.9% (**Figure 15c**). In reality, the difference in the fabrication cost will be even greater if we consider the set-up costs and running costs. Moreover, the mechanical properties of the PSCs where both electrodes were SWNTs were superior to those of the single-SWNT-electrode-based PSCs, especially in terms of flexibility. Subsequently, Luo *et al*., reported PSCs with both carbon electrodes being carbon-based; they used a CNT anode and a graphene cathode.[198] Their dual-carbon-electrode PSCs produced a PCE of 11.9% (**Table 3: Device U**). The high performance came from the fact that they adopted a normal architecture for the PSCs, and highly transparent single-layered graphene was used as the front electrode. Their flexible PSCs

with both electrodes being carbon-based demonstrate superior mechanical robustness against bending cycles at a curvature radius of 4 mm in comparison with ITO-based control devices. The flexible PSCs with both electrodes being carbon-based retained 86% of their original PCEs even after 2000 bending cycles. The identity of the CNT back electrode they used is not fully described; however, we conjecture that it employed multi-walled CNTs from their *ca.* 10 nm-thick-diameter.[199] Such an all-carbon concept will open up new avenues for versatile applications of carbon.

4. Conclusion

Up to this point, we have looked into the applications of SWNTs as transparent electrodes in the emerging thin-film solar cells. This review touched on the syntheses of SWNT electrodes and went over their applications in organic solar cells, DSSCs, and PSCs. By looking at the research direction of the SWNT-electrode photovoltaic applications, it is clear that the SWNT-electrode replacement is extended to dual CNT electrode systems in which CNTs are used as a pair, or in a combination with other carbon electrodes. It is our prediction that the application of CNT electrodes will be extended to tandem devices.[200] Considering this trend, there is no doubt that the excellent properties of SWNTs give them the potential to become the next-generation electrode for photovoltaic devices. Here, we would like to conclude this review by going through five key aspects of SWNT electrodes that should be worked on to ensure their viability in emerging thin-film photovoltaics.

The first aspect is that the synthesis and fabrication of SWNTs can and should be made easier. Currently, compared to past developments, the synthesis and the control of their properties have gotten somewhat easier.[201] As we discussed in section 2, for electrode use, it is important to obtain longer SWNTs with more consistent diameters. In addition, the SWNTs should be either fully metallic or a mixture of metallic and semiconducting. This means that the

chirality control of SWNTs is important. It is preferred that we want to develop fully metallic SWNTs for the electrode usage in OSCs, because charge selectivity of SWNTs plays little or no role in OSC devices. On the other hand, for the top electrode in PSCs, the charge selective function of SWNTs is equally important so that a mixture of metallic and semiconducting properties of SWNTs is desired. The orientation of the SWNTs is also important because most SWNT-electrode-based photovoltaics utilize randomly oriented SWNTs. To the best of our knowledge, VA- or HA-SWNT electrodes in emerging solar cells have not been demonstrated, unlike silicon solar cells. We expect such SWNTs with a specific orientation can also prove to be beneficial to OSCs and PSCs. In terms of the fabrication process, aerosol SWNT-electrodes already have the enormous advantage of being laminated,[157,190] which is much more promising for the large-size photovoltaic fabrication than the wet transfer of other carbon electrodes. However, this advantage can become even greater with the solution processing of CNT electrodes. The solution processability of CNT electrodes has already been successfully demonstrated by many groups as mentioned in this review (**Table 2**), but their performance is not quite as good as that of the laminated SWNTs. Further progress in the development of the solution-processed CNT electrodes can open up more opportunities for CNT-electrode-based photovoltaics. Effective removal of surfactants from solution-processed CNT electrodes can be one way to advance their performance while doping CNTs in their solution state can be another way. There are also crude, but effective, mechanical approaches. For example, overlaying CNT grids on top of CNT electrodes has been reported to boost the conductivity.[202,203] Capitalizing on the unique properties of double-walled CNTs is another viable option.[31,204] Double-walled CNTs are as transparent and conductive as SWNTs, yet manifest highly a dispersible nature, akin to MWNTs, that can lead to high-performance electrodes when spin-coated. Many challenges remain; however, there are many avenues to the next level of CNT electrodes.

Secondly, the dc to optical conductivity ratio of an electrode,[205] which is the transparency divided by the resistance is the factor that differentiates between ITO-based

photovoltaics and SWNT-based photovoltaics. Neither the transparency nor the conductivity of CNT electrodes is comparable to those of ITO or metals yet. While it is necessary to improve both the transparency and conductivity, it is important to give more attention to the conductivity at the expense of transparency if the SWNT electrode is not being used as the transparent electrode. Therefore, the conductivity is a more pressing limitation and the biggest bottleneck for SWNT electrodes.

We can improve the conductivity either by focusing on the synthesis level of SWNTs, or by relying on post-treatments, such as dopants. One of the ways to improve the synthesis process itself would be to remove metal catalysts, because the metal particles have no function after the growth process. An easier approach, however, would be to use *p*-dopants. Many papers have already been published reporting on stable and effective dopants for carbon electrodes. Recently polymeric acid, which is as effective as the conventional acidic dopants but shows almost immeasurable durability time has been discovered. Likewise, there are countless materials to be explored that can potentially function as effective and stable dopants.

Energy level alignment is the third point to consider. The Fermi level of the CNT plays a crucial role in achieving high-performance photovoltaics. In general, carbon electrodes have been reported to have Fermi levels of –4.5 to –5 eV. The Fermi level can be tuned by various dopants. Materials like acids and PEDOT:PSS will *p*-dope CNTs, decreasing the values of the Fermi level. Strong acids like HNO_3 and TFMS can shift the Fermi level to more than –6.0 eV. As discussed in the previous section,[171,179] the energy level matching between the Fermi level of CNTs and the valence band of perovskite is an important factor that determines V_{OC}. Fine tuning of the energy level by means of effective and stable doping is a worthwhile research topic for the future. For the CNT cathodes, obtaining the right Fermi level to minimize energy barriers is particularly crucial–much more than for the CNT anodes. Cs_2CO_3 and PCBM are two of the examples of *n*-dopants used to reduce the Fermi level for electron collection at the cathode.[190] Carbon cathodes have not been studied as much as the anodes; hence, this is also

a fascinating and important area to explore, especially for the development of all-carbon solar cells.

The surface properties are the fourth point. Wettability is an essential factor in solar cell fabrication. The fact that CNT electrodes are hydrophobic limits the type of materials that can be deposited on top and the deposition methodology as well. Therefore, controlling the surface energy of CNT electrodes can directly impact the cost and ease of the fabrication process. There are numerous chemical treatments that enable this. In many cases, these treatments also have a doping effect. Therefore, it is possible to control both wettability and Fermi level at the same time. Further, the intrinsic surface roughness of CNTs affects the device performance and reproducibility.[183] Hence, more attention should be paid to the surface morphology improvement either by controlling the growth process of SWNTs or by post-treatments. Again, various dopants can overcoat the SWNTs to fill in the network. Materials like polymers are particularly effective for this.[169]

Lastly, the functionality of SWNTs has not been fully explored. The flexibility aspect is already well known; there is no question about their mechanical resilience, and SWNTs were found to be more flexible than even single-layered graphene (**Table 3: Device P and Q**).[183] However, there are other traits that we have not yet investigated. For example, it has been only recently demonstrated that the inertness of SWNTs leads to enhanced stability compared to metal electrodes that cause ion migration (**Table 3: Device G**).[161] Furthermore, researchers have overlooked the merit of SWNTs as a moisture and air barrier, which means that SWNTs can serve an excellent encapsulating function (**Table 3: Device J**).[169] For thin-film photovoltaics, stability under ambient conditions is vital for commercialization. The photoactive materials of these type of cells are rather unstable in air, and the barrier properties of plastic encapsulation are simply not good enough. Therefore, it is necessary to develop a flexible barrier that can passivate the device effectively. CNTs have shown some promise in

this regard, yet the current research in this area has not been sufficient. Further study will surely lead to the pathway to air-stable thin-film solar cell devices.

As reviewed above, substitution of electrodes plays a crucial role in the emerging thin-film solar devices and has been the subject of much research, which continues to this day. With the improvement on the properties of SWNTs at both synthesis and engineering levels, we can expect remarkable continuing advancement in the solar cell research. We have no doubt that there is still room for improvement to expedite this carbon-electrode research.

Acknowledgements

IJ and RX contributed equally to this work. IJ thanks the Research and Education Consortium for Innovation of Advanced Integrated Science by Japan Science and Technology (JST). A.S thanks Japan Society for the Promotion of Science (JSPS) Grant-in-Aid (17F17364) for financial support. This work was supported by JSPS KAKENHI Grant Numbers JP15H05760, JP17H06609, JP18H05329.

Received: ((will be filled in by the editorial staff))
Revised: ((will be filled in by the editorial staff))
Published online: ((will be filled in by the editorial staff))

References

[1] C. J. Brabec, S. Gowrisanker, J. J. M. Halls, D. Laird, S. Jia, S. P. Williams, *Adv. Mater.* **2010**, *22*, 3839.

[2] I. Jeon, Y. Matsuo, in *Encycl. Polym. Sci. Technol.*, John Wiley & Sons, Inc., Hoboken, NJ, USA, **2017**, 1-21.

[3] G. Li, R. Zhu, Y. Yang, *Nat. Photonics* **2012**, *6*, 153.

[4] J.-P. Correa-Baena, M. Saliba, T. Buonassisi, M. Grätzel, A. Abate, W. Tress, A. Hagfeldt, *Science* **2017**, *358*, 739.

[5] M. A. Green, A. Ho-Baillie, H. J. Snaith, *Nat. Photonics* **2014**, *8*, 506.

[6] F. Di Giacomo, A. Fakharuddin, R. Jose, T. M. Brown, *Energy Environ. Sci.* **2016**, *9*, 3007.

[7] L. Zuo, C. Chueh, Y. Xu, K.-S. Chen, Y. Zang, C. Li, H. Chen, A. K.-Y. Jen, *Adv. Mater.* **2014**, *26*, 6778.

[8] K. A. Bush, A. F. Palmstrom, Z. J. Yu, M. Boccard, R. Cheacharoen, J. P. Mailoa, D. P. McMeekin, R. L. Z. Hoye, C. D. Bailie, T. Leijtens, I. M. Peters, M. C. Minichetti, N. Rolston, R. Prasanna, S. Sofia, D. Harwood, W. Ma, F. Moghadam, H. J. Snaith, T. Buonassisi, Z. C. Holman, S. F. Bent, M. D. McGehee, *Nat. Energy* **2017**, *2*, 17009.

[9] Y. Liu, Z. Hong, Q. Chen, W. Chang, H. Zhou, T.-B. Song, E. Young, Y. (Michael) Yang, J. You, G. Li, Y. Yang, *Nano Lett.* **2015**, *15*, 662.

[10] K. Gao, Z. Zhu, B. Xu, S. B. Jo, Y. Kan, X. Peng, A. K. Y. Jen, *Adv. Mater.* **2017**, *29*, 1703980.

[11] S. Iijima, T. Ichihashi, *Nature* **1993**, *363*, 603.

[12] Z. Li, H. R. Kandel, E. Dervishi, V. Saini, A. S. Biris, A. R. Biris, D. Lupu, *Appl. Phys. Lett.* **2007**, *91*, 53115.

[13] J. Du, S. Pei, L. Ma, H.-M. Cheng, *Adv. Mater.* **2014**, *26*, 1958.

[14] U. N. Maiti, W. J. Lee, J. M. Lee, Y. Oh, J. Y. Kim, J. E. Kim, J. Shim, T. H. Han, S. O. Kim, *Adv. Mater.* **2014**, *26*, 40.

[15] D.-M. Sun, C. Liu, W.-C. Ren, H.-M. Cheng, *Small* **2013**, *9*, 1188.

[16] I. Jeon, Y. Matsuo, S. Maruyama, *Top. Curr. Chem.* **2018**, *376*, 4.

[17] H. Dai, A. G. Rinzler, P. Nikolaev, A. Thess, D. T. Colbert, R. E. Smalley, *Chem. Phys. Lett.* **1996**, *260*, 471.

[18] J. Kong, A. M. Cassell, H. Dai, *Chem. Phys. Lett.* **1998**, *292*, 567.

[19] L. Yu, C. Shearer, J. Shapter, *Chem. Rev.* **2016**, *116*, 13413.

[20] A. Thess, R. Lee, P. Nikolaev, H. Dai, P. Petit, J. Robert, C. Xu, Y. H. Lee, S. G. Kim, A. G. Rinzler, D. T. Colbert, G. E. Scuseria, D. Tomanek, J. E. Fischer, R. E. Smalley, *Science* **1996**, *273*, 483.

[21] A. Moisala, A. G. Nasibulin, D. P. Brown, H. Jiang, L. Khriachtchev, E. I. Kauppinen,

Chem. Eng. Sci. **2006**, *61*, 4393.

[22] I. W. Chiang, B. E. Brinson, A. Y. Huang, P. A. Willis, M. J. Bronikowski, J. L. Margrave, R. E. Smalley, R. H. Hauge, *J. Phys. Chem. B* **2001**, *105*, 8297.

[23] R. L. Carver, H. Peng, A. K. Sadana, P. Nikolaev, S. Arepalli, C. D. Scott, W. E. Billups, R. H. Hauge, R. E. Smalley, *J. Nanosci. Nanotechnol.* **2005**, *5*, 1035.

[24] G. I. Koleilat, L. Levina, H. Shukla, S. H. Myrskog, S. Hinds, A. G. Pattantyus-Abraham, E. H. Sargent, *ACS Nano* **2008**, *2*, 833.

[25] S. M. Bachilo, L. Balzano, J. E. Herrera, F. Pompeo, D. E. Resasco, R. B. Weisman, *J. Am. Chem. Soc.* **2003**, *125*, 11186.

[26] S. Maruyama, R. Kojima, Y. Miyauchi, S. Chiashi, M. Kohno, *Chem. Phys. Lett.* **2002**, *360*, 229.

[27] Y. Murakami, Y. Miyauchi, S. Chiashi, S. Maruyama, *Chem. Phys. Lett.* **2003**, 374, 53.

[28] H. M. Cheng, F. Li, G. Su, H. Y. Pan, L. L. He, X. Sun, M. S. Dresselhaus, *Appl. Phys. Lett.* **1998**, *72*, 3282.

[29] J. H. Du, S. F. Pei, L. P. Ma, H. M. Cheng, *Adv. Mater.* **2014**, 26, 1958.

[30] S. Jiang, P. X. Hou, M. L. Chen, B. W. Wang, D. M. Sun, D. M. Tang, Q. Jin, Q. X. Guo, D. D. Zhang, J. H. Du, K. P. Tai, J. Tan, E. I. Kauppinen, C. Liu, H. M. Cheng, *Sci. Adv.* **2018**, 4, eaap9264.

[31] T. Saito, S. Ohshima, T. Okazaki, S. Ohmori, M. Yumura, S. Iijima, *J. Nanosci. Nanotechnol.* **2008**, *8*, 6153.

[32] "eDIPS AIST press release," can be found under http://www.aist.go.jp/aist_j/press_release/pr2013/pr20131224/pr20131224.html., **n.d.**

[33] T. Saito, W.-C. Xu, S. Ohshima, H. Ago, M. Yumura, S. Iijima, *J. Phys. Chem. B* **2006**, *110*, 5849.

[34] B. Shukla, T. Saito, M. Yumura, S. Iijima, *Chem. Commun.* **2009**, 3422.

[35] A. G. Nasibulin, A. Kaskela, K. Mustonen, A. S. Anisimov, V. Ruiz, S. Kivistö, S.

Rackauskas, M. Y. Timmermans, M. Pudas, B. Aitchison, M. Kauppinen, D. P. Brown, O. G. Okhotnikov, E. I. Kauppinen, *ACS Nano* **2011**, *5*, 3214.

[36] E. X. Ding, H. Jiang, Q. Zhang, Y. Tian, P. Laiho, A. Hussain, Y. P. Liao, N. Wei, E. I. Kauppinen, *Nanoscale* **2017**, 9, 17601.

[37] Y. Tian, M. Y. Timmermans, M. Partanen, A. G. Nasibulin, H. Jiang, Z. Zhu, E. I. Kauppinen, *Carbon* **2011**, *49*, 4636.

[38] K. Mustonen, P. Laiho, A. Kaskela, T. Susi, A. G. Nasibulin, E. I. Kauppinen, *Appl. Phys. Lett.* **2015**, *107*, 143113.

[39] A. Kaskela, P. Laiho, N. Fukaya, K. Mustonen, T. Susi, H. Jiang, N. Houbenov, Y. Ohno, E. I. Kauppinen, *Carbon* **2016**, 103, 228.

[40] Y. P. Liao, H. Jiang, N. Wei, P. Laiho, Q. Zhang, S. A. Khan, E. I. Kauppinen, *J. Am. Chem. Soc.* **2018**, 140, 9797.

[41] D. Ciuparu, Y. Chen, S. Lim, G. L. Haller, L. Pfefferle, *J. Phys. Chem. B* **2004**, *108*, 503.

[42] G. Ning, F. Wei, Q. Wen, G. Luo, Y. Wang, Y. Jin, *J. Phys. Chem. B* **2006**, *110*, 1201.

[43] B. Hou, C. Wu, T. Inoue, S. Chiashi, R. Xiang, S. Maruyama, *Carbon* **2017**, *119*, 502.

[44] Y. Murakami, S. Chiashi, Y. Miyauchi, M. Hu, M. Ogura, T. Okubo, S. Maruyama, *Chem. Phys. Lett.* **2004**, *385*, 298.

[45] Y. Miyauchi, S. Chiashi, Y. Murakami, Y. Hayashida, S. Maruyama, *Chem. Phys. Lett.* **2004**, *387*, 198.

[46] K. Hata, D. N. Futaba, K. Mizuno, T. Namai, M. Yumura, S. Iijima, *Science* **2004**, 306, 1362.

[47] "Zeon Mass Production of CNT Press Release," can be found under http://www.zeon.co.jp/press_e/140515.html

[48] D. N. Futaba, K. Hata, T. Yamada, K. Mizuno, M. Yumura, S. Iijima, *Phys. Rev. Lett.* **2005**, *95*, 56104.

[49] E. Einarsson, Y. Murakami, M. Kadowaki, S. Maruyama, *Carbon* **2008**, *46*, 923.

[50] Y. Murakami, E. Einarsson, T. Edamura, S. Maruyama, *Phys. Rev. Lett.* **2005**, *94*, 87402.

[51] C.-T. Lin, C.-Y. Lee, T.-S. Chin, R. Xiang, K. Ishikawa, J. Shiomi, S. Maruyama, *Carbon* **2011**, *49*, 1446.

[52] C. L. Pint, Y.-Q. Xu, S. Moghazy, T. Cherukuri, N. T. Alvarez, E. H. Haroz, S. Mahzooni, S. K. Doorn, J. Kono, M. Pasquali, R. H. Hauge, *ACS Nano* **2010**, *4*, 1131.

[53] R. Xiang, T. Wu, E. Einarsson, Y. Suzuki, Y. Murakami, J. Shiomi, S. Maruyama, *J. Am. Chem. Soc.* **2009**, *131*, 10344.

[54] R. Xiang, E. Einarsson, H. Okabe, S. Chiashi, J. Shiomi, S. Maruyama, *Jpn J. Appl. Phys.* **2010**, 49.

[55] R. Xiang, E. Einarsson, Y. Murakami, J. Shiomi, S. Chiashi, Z. Tang, S. Maruyama, *ACS Nano* **2012**, *6*, 7472.

[56] G. Chen, Y. Seki, H. Kimura, S. Sakurai, M. Yumura, K. Hata, D. N. Futaba, *Sci. Rep.* **2015**, *4*, 3804.

[57] K. Cui, A. Kumamoto, R. Xiang, H. An, B. Wang, T. Inoue, S. Chiashi, Y. Ikuhara, S. Maruyama, *Nanoscale* **2016**, *8*, 1608.

[58] J. K. Holt, H. G. Park, Y. Wang, M. Stadermann, A. B. Artyukhin, C. P. Grigoropoulos, A. Noy, O. Bakajin, *Science* **2006**, *312*, 1034.

[59] K. Cui, T. Chiba, S. Omiya, T. Thurakitseree, P. Zhao, S. Fujii, H. Kataura, E. Einarsson, S. Chiashi, S. Maruyama, *J. Phys. Chem. Lett.* **2013**, *4*, 2571.

[60] L. X. Zheng, M. J. O'Connell, S. K. Doorn, X. Z. Liao, Y. H. Zhao, E. A. Akhadov, M. A. Hoffbauer, B. J. Roop, Q. X. Jia, R. C. Dye, D. E. Peterson, S. M. Huang, J. Liu, Y. T. Zhu, *Nat. Mater.* **2004**, *3*, 673.

[61] S. Huang, M. Woodson, R. Smalley, J. Liu, *Nano Lett.* **2004**, *4*, 1025.

[62] Z. Jin, H. Chu, J. Wang, J. Hong, W. Tan, Y. Li, *Nano Lett.* **2007**, *7*, 2073.

[63] Q. Wen, W. Qian, J. Nie, A. Cao, G. Ning, Y. Wang, L. Hu, Q. Zhang, J. Huang, F. Wei, *Adv. Mater.* **2010**, *22*, 1867.

[64] R. Zhang, Y. Zhang, Q. Zhang, H. Xie, W. Qian, F. Wei, *ACS Nano* **2013**, *7*, 6156.

[65] Y. X. Bai, R. F. Zhang, X. Ye, Z. X. Zhu, H. H. Xie, B. Y. Shen, D. L. Cai, B. F. Liu, C. X. Zhang, Z. Jia, S. L. Zhang, X. D. Li, F. Wei, *Nat. Nanotechnol.* **2018**, 13, 589.

[66] R. F. Zhang, Y. Y. Zhang, F. Wei, *Accounts Chem. Res.* **2017**, 50, 179.

[67] A. Ismach, L. Segev, E. Wachtel, E. Joselevich, *Angew. Chemie Int. Ed.* **2004**, *43*, 6140.

[68] S. Han, X. Liu, C. Zhou, *J. Am. Chem. Soc.* **2005**, *127*, 5294.

[69] C. Kocabas, S.-H. Hur, A. Gaur, M. A. Meitl, M. Shim, J. A. Rogers, *Small* **2005**, *1*, 1110.

[70] K. Otsuka, T. Inoue, E. Maeda, R. Kometani, S. Chiashi, S. Maruyama, *ACS Nano* **2017**, 11, 11497.

[71] Y. Hu, L. Kang, Q. Zhao, H. Zhong, S. Zhang, L. Yang, Z. Wang, J. Lin, Q. Li, Z. Zhang, L. Peng, Z. Liu, J. Zhang, *Nat. Commun.* **2015**, *6*, 6099.

[72] M. M. Shulaker, G. Hills, N. Patil, H. Wei, H.-Y. Chen, H.-S. P. Wong, S. Mitra, *Nature* **2013**, *501*, 526.

[73] J. T. Wang, X. JIn, Z. Liu, G. Yu, Q. Ji, H. Wei, J. Zhang, K. Zhang, D. Li, Z. Yuan, J. Li, P. Liu, Y. Wu, Y. Wei, J. Wang, Q. Li, L. Zhang, J. Kong, S. Fan, K. L. Jiang, *Nat. Catalysis* **2018**, 1, 326.

[74] J. T. Wang, T. Y. Li, B. Y. Xia, X. Jin, H. M. Wei, W. Y. Wu, Y. Wei, J. P. Wang, P. Liu, L. N. Zhang, Q. Q. Li, S. S. Fan, K. L. Jiang, *Nano Lett.* **2014**, 14, 3527.

[75] J. T. Wang, P. Liu, B. Y. Xia, H. M. Wei, Y. Wei, Y. Wu, K. Liu, L. N. Zhang, J. P. Wang, Q. Q. Li, S. S. Fan, K. L. Jiang, *Nano Lett.* **2016**, 16, 4102.

[76] D. Q. Li, J. Zhang, Y. J. He, Y. Qin, Y. Wei, P. Liu, L. N. Zhang, J. P. Wang, Q. Q. Li, S. S. Fan, K. L. Jiang, *Nano Res.* **2017**, 10, 1804.

[77] X. L. Zhao, S. C. Zhang, Z. X. Zhu, J. Zhang, F. Wei, Y. Li, *MRS Bulletin* **2017**, 42, 809.

[78] F. Yang, X. Wang, D. Zhang, J. Yang, D. Luo, Z. Xu, J. Wei, J.-Q. Wang, Z. Xu, F. Peng, X. Li, R. Li, Y. Li, M. Li, X. Bai, F. Ding, Y. Li, *Nature* **2014**, *510*, 522.

[79] F. Yang, X. Wang, J. Si, X. Zhao, K. Qi, C. Jin, Z. Zhang, M. Li, D. Zhang, J. Yang, Z. Zhang, Z. Xu, L.-M. Peng, X. Bai, Y. Li, *ACS Nano* **2017**, *11*, 186.

[80] F. Yang, X. Wang, M. Li, X. Liu, X. Zhao, D. Zhang, Y. Zhang, J. Yang, Y. Li, *Acc. Chem. Res.* **2016**, *49*, 606.

[81] H. An, A. Kumamoto, H. Takezaki, S. Ohyama, Y. Qian, T. Inoue, Y. Ikuhara, S. Chiashi, R. Xiang, S. Maruyama, *Nanoscale* **2016**, *8*, 14523.

[82] S. Zhang, L. Kang, X. Wang, L. Tong, L. Yang, Z. Wang, K. Qi, S. Deng, Q. Li, X. Bai, F. Ding, J. Zhang, *Nature* **2017**, *543*, 234.

[83] Y. Yuan, H. E. Karahan, C. Yildirim, L. Wei, O. Birer, S. L. Zhai, R. Lau, Y. Chen, *Nanoscale* **2016**, 8, 17705.

[84] H. Wang, L. Yang, X. Sui, H. E. Karahan, X. L. Wang, Y. Chen, *Carbon* **2018**, 129, 128.

[85] H. Wang, L. Wei, F. Ren, Q. Wang, L. D. Pfefferle, G. L. Haller, Y. Chen, *ACS Nano* **2013**, 7, 614.

[86] H. Wang, F. Ren, C. C. Liu, R. M. Si, D. S. Yu, L. D. Pfefferle, G. L. Haller, Y. Chen, *J Catal.* **2013**, 300, 91.

[87] B. Xu, T. Kaneko, Y. Shibuta, T. Kato, *Sci. Rep.* **2017**, 7.

[88] Y. G. Yao, C. Q. Feng, J. Zhang, Z. F. Liu, *Nano Lett.* **2009**, 9, 1673.

[89] D. W. Lin, S. C. Zhang, Z. Zheng, W. P. Hu, J. Zhang, *Small* **2018**, 14.

[90] J. Liu, C. Wang, X. M. Tu, B. L. Liu, L. Chen, M. Zheng, C. W. Zhou, *Nat. Commun.* **2012**, 3.

[91] B. L. Liu, J. Liu, X. M. Tu, J. L. Zhang, M. Zheng, C. W. Zhou, *Nano Lett* **2013**, 13,

4416.

[92] H. Omachi, T. Nakayama, E. Takahashi, Y. Segawa, K. Itami, *Nat. Chem.* **2013**, 5, 572.

[93] H. Omachi, Y. Segawa, K. Itami, *Accounts Chem. Res.* **2012**, 45, 1378.

[94] G. Povie, Y. Segawa, T. Nishihara, Y. Miyauchi, K. Itami, *Science* **2017**, 356, 172.

[95] N. Pierce, G. Chen, L. P. Rajukumar, N. H. Chou, A. L. Koh, R. Sinclair, S. Maruyama, M. Terrones, A. R. Harutyunyan, *ACS Nano* **2017**, *11*, 9941.

[96] R. Xiang, S. Maruyama, *R. Soc. Open Sci.* **2018**, 5, 180345.

[97] Bianco, Y. S. Chen, Y. Chen, D. Ghoshal, R. H. Hurt, Y. A. Kim, N. Koratkar, V. Meunier, M. Terrones, *Carbon* **2018**, 132, 785.

[98] M. Cai, Y. Wu, H. Chen, X. Yang, Y. Qiang, L. Han, *Adv. Sci.* **2017**, *4*, 1600269.

[99] B. J. Kim, D. H. Kim, Y.-Y. Lee, H.-W. Shin, G. S. Han, J. S. Hong, K. Mahmood, T. K. Ahn, Y.-C. Joo, K. S. Hong, N.-G. Park, S. Lee, H. S. Jung, *Energy Environ. Sci.* **2015**, *8*, 916.

[100] K. Zilberberg, F. Gasse, R. Pagui, A. Polywka, A. Behrendt, S. Trost, R. Heiderhoff, P. Görrn, T. Riedl, *Adv. Funct. Mater.* **2014**, *24*, 1671.

[101] O. Inganäs, *Nat. Photonics* **2011**, *5*, 201.

[102] M. Yang, D. Kim, H. Jha, K. Lee, J. Paul, P. Schmuki, *Chem. Commun.* **2011**, *47*, 2032.

[103] C. Delacou, I. Jeon, S. Seo, T. Nakagawa, E. I. Kauppinen, S. Maruyama, Y. Matsuo, *ECS J. Solid State Sci. Technol.* **2017**, *6*, M3181.

[104] I. Jeon, S. Nakao, Y. Hirose, T. Hasegawa, Y. Matsuo, *Adv. Electron. Mater.* **2016**, *2*, 1500341.

[105] Z. C. Wu, Z. H. Chen, X. Du, J. M. Logan, J. Sippel, M. Nikolou, K. Kamaras, J. R. Reynolds, D. B. Tanner, A. F. Hebard, A. G. Rinzler, *Science* **2004**, *305*, 1273.

[106] Y. H. Lee, S. G. Kim, D. Tománek, *Phys. Rev. Lett.* **1997**, *78*, 2393.

[107] J. van de Lagemaat, T. M. Barnes, G. Rumbles, S. E. Shaheen, T. J. Coutts, C. Weeks, I. Levitsky, J. Peltola, P. Glatkowski, *Appl. Phys. Lett.* **2006**, *88*, 233503.

[108] N. S. Sariciftci, L. Smilowitz, A. J. Heeger, F. Wudl, *Science* **1992**, *258*, 1474.

[109] G. Yu, J. Gao, J. C. Hummelen, F. Wudl, A. J. Heeger, *Science* **1995**, *270*, 1789.

[110] G. Dennler, M. C. Scharber, C. J. Brabec, *Adv. Mater.* **2009**, *21*, 1323.

[111] S. R. Forrest, *Nature* **2004**, *428*, 911.

[112] D. J. Lipomi, B. C.-K. Tee, M. Vosgueritchian, Z. Bao, *Adv. Mater.* **2011**, *23*, 1771.

[113] Y. Kim, J. Zhu, B. Yeom, M. Di Prima, X. Su, J.-G. Kim, S. J. Yoo, C. Uher, N. A. Kotov, *Nature* **2013**, *500*, 59.

[114] S. Berny, N. Blouin, A. Distler, H.-J. Egelhaaf, M. Krompiec, A. Lohr, O. R. Lozman, G. E. Morse, L. Nanson, A. Pron, T. Sauermann, N. Seidler, S. Tierney, P. Tiwana, M. Wagner, H. Wilson, *Adv. Sci.* **2016**, *3*, 1500342.

[115] I. Jeon, R. Sakai, S. Seo, G. E. Morse, H. Ueno, T. Nakagawa, Y. Qian, S. Maruyama, Y. Matsuo, *J. Mater. Chem. A* **2018**, *6*, 5746.

[116] S. Holliday, R. S. Ashraf, A. Wadsworth, D. Baran, S. A. Yousaf, C. B. Nielsen, C.-H. Tan, S. D. Dimitrov, Z. Shang, N. Gasparini, M. Alamoudi, F. Laquai, C. J. Brabec, A. Salleo, J. R. Durrant, I. McCulloch, *Nat. Commun.* **2016**, *7*, 11585.

[117] J. Hou, O. Inganäs, R. H. Friend, F. Gao, *Nat. Mater.* **2018**, *17*, 119.

[118] A. Du Pasquier, H. E. Unalan, A. Kanwal, S. Miller, M. Chhowalla, *Appl. Phys. Lett.* **2005**, *87*, 1.

[119] Y. Zhou, L. Hu, G. Grüner, *Appl. Phys. Lett.* **2006**, *88*, 123109.

[120] M. W. Rowell, M. A. Topinka, M. D. McGehee, H. Prall, G. Dennler, N. S. Sariciftci, L. Hu, G. Gruner, *Appl. Phys. Lett.* **2006**, *88*, 233506.

[121] H. E. Unalan, P. Hiralal, D. Kuo, B. Parekh, G. Amaratunga, M. Chhowalla, *J. Mater. Chem.* **2008**, *18*, 5909.

[122] E. Kymakis, G. Klapsis, E. Koudoumas, E. Stratakis, N. Kornilios, N. Vidakis, Y.

Franghiadakis, *Eur. Phys. J. Appl. Phys.* **2006**, *36*, 257.

[123] M. Kaltenbrunner, M. S. White, E. D. Głowacki, T. Sekitani, T. Someya, N. S. Sariciftci, S. Bauer, *Nat. Commun.* **2012**, *3*, 770.

[124] S. Kim, J. Yim, X. Wang, D. D. C. Bradley, S. Lee, J. C. DeMello, *Adv. Funct. Mater.* **2010**, *20*, 2310.

[125] T. P. Tyler, R. E. Brock, H. J. Karmel, T. J. Marks, M. C. Hersam, *Adv. Energy Mater.* **2011**, *1*, 785.

[126] M. S. Arnold, A. A. Green, J. F. Hulvat, S. I. Stupp, M. C. Hersam, *Nat. Nanotechnol.* **2006**, *1*, 60.

[127] R. V. Salvatierra, C. E. Cava, L. S. Roman, A. J. G. Zarbin, *Adv. Funct. Mater.* **2013**, *23*, 1490.

[128] H. Bejbouji, L. Vignau, J. L. Miane, M.-T. Dang, E. M. Oualim, M. Harmouchi, A. Mouhsen, *Sol. Energy Mater. Sol. Cells* **2010**, *94*, 176.

[129] B. H. Lee, S. H. Park, H. Back, K. Lee, *Adv. Funct. Mater.* **2011**, *21*, 487.

[130] M. C. Schnitzler, M. M. Oliveira, D. Ugarte, A. J. G. Zarbin, *Chem. Phys. Lett.* **2003**, *381*, 541.

[131] I. Jeon, K. Cui, T. Chiba, A. Anisimov, A. G. Nasibulin, E. I. Kauppinen, S. Maruyama, Y. Matsuo, *J. Am. Chem. Soc.* **2015**, *137*, 7982.

[132] E. Bundgaard, F. Krebs, *Sol. Energy Mater. Sol. Cells* **2007**, *91*, 954.

[133] S. L. Hellstrom, M. Vosgueritchian, R. M. Stoltenberg, I. Irfan, M. Hammock, Y. B. Wang, C. Jia, X. Guo, Y. Gao, Z. Bao, *Nano Lett.* **2012**, *12*, 3574.

[134] J. Roncali, P. Leriche, P. Blanchard, *Adv. Mater.* **2014**, *26*, 3821.

[135] S. D. Collins, N. A. Ran, M. C. Heiber, T. Nguyen, *Adv. Energy Mater.* **2017**, *7*, 1602242.

[136] I. Jeon, C. Delacou, A. Kaskela, E. I. Kauppinen, S. Maruyama, Y. Matsuo, *Sci. Rep.* **2016**, *6*, 31348.

[137] B. O'Regan, M. Grätzel, *Nature* **1991**, *353*, 737.

[138] F. Hao, P. Dong, Q. Luo, J. Li, J. Lou, H. Lin, *Energy Environ. Sci.,* **2013**, *6*, 2003.

[139] F. Hao, P. Dong, J. Zhang, Y. Zhang, P. E. Loya, R. H. Hauge, J. Li, J. Lou, H. Lin, *Sci. Rep.* **2012**, *2*, 368.

[140] S. Chappel, S.-G. Chen, A. Zaban, *Langmuir* **2002**, *18*, 3336.

[141] A. Kay, M. Grätzel, *Sol. Energy Mater. Sol. Cells* **1996**, *44*, 99.

[142] K. Suzuki, M. Yamaguchi, M. Kumagai, S. Yanagida, *Chem. Lett.* **2003**, *32*, 28.

[143] S.-R. Jang, R. Vittal, K.-J. Kim, *Langmuir* **2004**, *20*, 9807.

[144] A. Kongkanand, R. M. Domínguez, P. V. Kamat, *Nano Lett.* **2007**, *7*, 676.

[145] G. Li, F. Wang, Q. Jiang, X. Gao, P. Shen, *Angew. Chemie Int. Ed.* **2010**, *49*, 3653.

[146] H.-J. Shin, S. S. Jeon, S. S. Im, *Synth. Met.* **2011**, *161*, 1284.

[147] H. Anwar, A. E. George, I. G. Hill, *Sol. Energy* **2013**, *88*, 129.

[148] A. K. K. Kyaw, H. Tantang, T. Wu, L. Ke, J. Wei, H. V. Demir, Q. Zhang, X. W. Sun, *J. Phys. D-Appl. Phys.* **2012**, *45*, 165103.

[149] A. Kojima, K. Teshima, Y. Shirai, T. Miyasaka, *J. Am. Chem. Soc.* **2009**, *131*, 6050.

[150] H.-S. Kim, C.-R. Lee, J.-H. Im, K.-B. Lee, T. Moehl, A. Marchioro, S.-J. Moon, R. Humphry-Baker, J.-H. Yum, J. E. Moser, M. Grätzel, N.-G. Park, *Sci. Rep.* **2012**, *2*, 591.

[151] M. M. Lee, J. Teuscher, T. Miyasaka, T. N. Murakami, H. J. Snaith, *Science* **2012**, *338*, 643.

[152] J. Yoon, H. Sung, G. Lee, W. Cho, N. Ahn, H. S. Jung, M. Choi, *Energy Environ. Sci.* **2017**, *10*, 337.

[153] Y. Zhou, X. Yin, Q. Luo, X. Zhao, D. Zhou, J. Han, F. Hao, M. Tai, J. Li, P. Liu, K. Jiang, H. Lin, *ACS Appl. Mater. Interfaces* **2018** *10*, 31384.

[154] K. Domanski, J. P. Correa-Baena, N. Mine, M. K. Nazeeruddin, A. Abate, M. Saliba, W. Tress, A. Hagfeldt, M. Grätzel, *ACS Nano* **2016**, *10*, 6306.

[155] C. Eames, J. M. Frost, P. R. F. Barnes, B. C. O'Regan, A. Walsh, M. S. Islam, *Nat. Commun.* **2015**, *6*, 7497.

[156] N. Aristidou, C. Eames, I. Sanchez-Molina, X. Bu, J. Kosco, M. S. Islam, S. A. Haque, *Nat. Commun.* **2017**, *8*, 15218.

[157] Z. Li, S. A. Kulkarni, P. P. Boix, E. Shi, A. Cao, K. Fu, S. K. Batabyal, J. Zhang, Q. Xiong, L. H. Wong, N. Mathews, S. G. Mhaisalkar, *ACS Nano* **2014**, *8*, 6797.

[158] X. Wang, Z. Li, W. Xu, S. A. Kulkarni, S. K. Batabyal, S. Zhang, A. Cao, L. H. Wong, *Nano Energy* **2015**, *11*, 728.

[159] K. Aitola, K. Sveinbjörnsson, J.-P. Correa-Baena, A. Kaskela, A. Abate, Y. Tian, E. M. J. Johansson, M. Grätzel, E. I. Kauppinen, A. Hagfeldt, G. Boschloo, *Energy Environ. Sci.* **2016**, *9*, 461.

[160] N. J. Jeon, J. H. Noh, W. S. Yang, Y. C. Kim, S. Ryu, J. Seo, S. Il Seok, *Nature* **2015**, *517*, 476.

[161] K. Aitola, K. Domanski, J.-P. Correa-Baena, K. Sveinbjörnsson, M. Saliba, A. Abate, M. Grätzel, E. Kauppinen, E. M. J. Johansson, W. Tress, A. Hagfeldt, G. Boschloo, *Adv. Mater.* **2017**, *29*, 1606398.

[162] M. O. Reese, S. A. Gevorgyan, M. Jørgensen, E. Bundgaard, S. R. Kurtz, D. S. Ginley, D. C. Olson, M. T. Lloyd, P. Morvillo, E. A. Katz, A. Elschner, O. Haillant, T. R. Currier, V. Shrotriya, M. Hermenau, M. Riede, K. R. Kirov, G. Trimmel, T. Rath, O. Inganäs, F. Zhang, M. Andersson, K. Tvingstedt, M. Lira-Cantu, D. Laird, C. McGuiness, S. (Jimmy) Gowrisanker, M. Pannone, M. Xiao, J. Hauch, R. Steim, D. M. DeLongchamp, R. Rösch, H. Hoppe, N. Espinosa, A. Urbina, G. Yaman-Uzunoglu, J.-B. Bonekamp, A. J. J. M. van Breemen, C. Girotto, E. Voroshazi, F. C. Krebs, *Sol. Energy Mater. Sol. Cells* **2011**, *95*, 1253.

[163] C. V. V. M. Gopi, M. Venkata-Haritha, K. Prabakar, H. J. Kim, *J. Photochem. Photobiol. A Chem.* **2017**, *332*, 265.

[164] J. Ryu, K. Lee, J. Yun, H. Yu, J. Lee, J. Jang, *Small* **2017**, *13*, 1701225.

[165] N. Ahn, K. Kwak, M. S. Jang, H. Yoon, B. Y. Lee, J. Lee, P. V Pikhitsa, J. Byun, M. Choi, *Nat. Commun.* **2016**, *7*, 13422.

[166] X. Zhao, H.-S. Kim, J.-Y. Seo, N.-G. Park, *ACS Appl. Mater. Interfaces* **2017**, *9*, 7148.

[167] A. K. Jena, Y. Numata, M. Ikegami, T. Miyasaka, *J. Mater. Chem. A* **2018**, *6*, 2219.

[168] T. Malinauskas, D. Tomkute-Luksiene, R. Sens, M. Daskeviciene, R. Send, H. Wonneberger, V. Jankauskas, I. Bruder, V. Getautis, *ACS Appl. Mater. Interfaces* **2015**, *7*, 11107.

[169] N. Ahn, I. Jeon, J. Yoon, E. I. Kauppinen, Y. Matsuo, S. Maruyama, M. Choi, *J. Mater. Chem. A* **2018**, *6*, 1382.

[170] H. W. Lee, Y. Yoon, S. Park, J. H. Oh, S. Hong, L. S. Liyanage, H. Wang, S. Morishita, N. Patil, Y. J. Park, J. J. Park, A. Spakowitz, G. Galli, F. Gygi, P. H.-S. Wong, J. B.-H. Tok, J. M. Kim, Z. Bao, *Nat. Commun.* **2011**, *2*, 541.

[171] J. Lee, I. Jeon, H. Lin, S. Seo, T.-H. Han, Y. Matsuo, S. Maruyama, Y. Yang, *Nano Lett.* **2018** in print.

[172] W. Shockley, H. J. Queisser, *J. Appl. Phys.* **1961**, *32*, 510.

[173] J.-W. Lee, Z. Dai, T.-H. Han, C. Choi, S.-Y. Chang, S.-J. Lee, N. D. Marco, H. Zhao, P. Sun, Y. Huang, Y. Yang, *Nature Commun.* **2018**, *9*, 3021.

[174] I. Jeon, C. Delacou, H. Okada, G. E. Morse, T.-H Han, Y. Sato, A. Anisimov, K. Suenaga, E. I. Kauppinen, S. Maruyama, Y. Matsuo, *J. Mater. Chem. A.* **2018**, *6*, 14553.

[175] L. Cojocaru, S. Uchida, P. V. V. Jayaweera, S. Kaneko, J. Nakazaki, T. Kubo, H. Segawa, *Chem. Lett.* **2015**, *44*, 1750.

[176] Z. Tang, T. Bessho, F. Awai, T. Kinoshita, M. M. Maitani, R. Jono, T. N. Murakami, H. Wang, T. Kubo, S. Uchida, H. Segawa, *Sci. Rep.* **2017**, *7*, 12183.

[177] Q. Jiang, L. Zhang, H. Wang, X. Yang, J. Meng, H. Liu, Z. Yin, J. Wu, X. Zhang, J.

You, *Nat. Energy* **2016**, *2*, 16177.

[178] K.-H. Jung, J.-Y. Seo, S. Lee, H. Shin, N.-G. Park, *J. Mater. Chem. A* **2017**, *5*, 24790.

[179] I. Jeon, T. Chiba, C. Delacou, Y. Guo, A. Kaskela, O. Reynaud, E. I. Kauppinen, S. Maruyama, Y. Matsuo, *Nano Lett.* **2015**, *15*, 6665.

[180] P. Liu, X. Liu, L. Lyu, H. Xie, H. Zhang, D. Niu, H. Huang, C. Bi, Z. Xiao, J. Huang, Y. Gao, *Appl. Phys. Lett.* **2015**, *106*, 193903.

[181] C. Wang, I. Irfan, X. Liu, Y. Gao, *J. Vac. Sci. Technol. B* **2014**, *32*, 40801.

[182] H. Sung, N. Ahn, M. S. Jang, J. Lee, H. Yoon, N. Park, M. Choi, *Adv. Energy Mater.* **2016**, *6*, 1501873.

[183] I. Jeon, J. Yoon, N. Ahn, M. Atwa, C. Delacou, A. Anisimov, E. I. Kauppinen, M. Choi, S. Maruyama, Y. Matsuo, *J. Phys. Chem. Lett.* **2017**, *8*, 5395.

[184] M. A. Bissett, W. Izumida, R. Saito, H. Ago, *ACS Nano* **2012**, *6*, 10229.

[185] D. L. Duong, G. H. Han, S. M. Lee, F. Gunes, E. S. Kim, S. T. Kim, H. Kim, Q. H. Ta, K. P. So, S. J. Yoon, S. H. S. J. Chae, Y. W. Jo, M. H. Park, S. H. S. J. Chae, S. C. Lim, J. Y. Choi, Y. H. Lee, *Nature* **2012**, *490*, 235.

[186] Q. Yu, L. A. Jauregui, W. Wu, R. Colby, J. Tian, Z. Su, H. Cao, Z. Liu, D. Pandey, D. Wei, T. F. Chung, P. Peng, N. P. Guisinger, E. A. Stach, J. Bao, S.-S. Pei, Y. P. Chen, *Nat. Mater.* **2011**, *10*, 443.

[187] T. M. G. Mohiuddin, A. Lombardo, R. R. Nair, A. Bonetti, G. Savini, R. Jalil, N. Bonini, D. M. Basko, C. Galiotis, N. Marzari, K. S. Novoselov, A. K. Geim, A. C. Ferrari, *Phys. Rev. B* **2009**, *79*, 205433.

[188] A. C. Ferrari, J. Robertson, *Phys. Rev. B* **2000**, *61*, 14095.

[189] L. M. Malard, M. A. Pimenta, G. Dresselhaus, M. S. Dresselhaus, *Phys. Rep.* **2009**, *473*, 51.

[190] I. Jeon, S. Seo, Y. Sato, C. Delacou, A. Anisimov, K. Suenaga, E. I. Kauppinen, S. Maruyama, Y. Matsuo, *J. Phys. Chem. C* **2017**, *121*, 25743.

[191] D. S. Cochran, J. F. Arinez, J. W. Duda, J. Linck, *J. Manuf. Syst.* **2002**, *20*, 371.

[192] T. T. Larsen-Olsen, R. R. Søndergaard, K. Norrman, M. Jørgensen, F. C. Krebs, *Energy Environ. Sci.* **2012**, *5*, 9467.

[193] K. Robinson, W. Durkin, *IEEE Trans. Ind. Appl.* **2010**, *46*, 2172.

[194] T.-J. Ha, K. Chen, S. Chuang, K. M. Yu, D. Kiriya, A. Javey, *Nano Lett.* **2015**, *15*, 392.

[195] T. Yasunishi, S. Kishimoto, Y. Ohno, *Jpn. J. Appl. Phys.* **2014**, *53*, 05FD01.

[196] N. A. M. Barakat, M. Shaheer Akhtar, I. M. A. Mohamed, Y. A. Dakka, R. Hamdan, A. G. El-Deen, K. Elsaid, M. Obaid, S. Al-Meer, *Mater. Lett.* **2017**, *191*, 80.

[197] N. Ahn, D.-Y. Son, I.-H. Jang, S. M. Kang, M. Choi, N. Park, *J. Am. Chem. Soc.* **2015**, *137*, 8696.

[198] Q. Luo, H. Ma, Q. Hou, Y. Li, J. Ren, X. Dai, Z. Yao, Y. Zhou, L. Xiang, H. Du, H. He, N. Wang, K. Jiang, H. Lin, H. Zhang, Z. Guo, *Adv. Funct. Mater.* **2018**, *28*, 1706777.

[199] K. Jiang, Q. Li, S. Fan, *Nature* **2002**, *419*, 801.

[200] S. Tanaka, K. Mielczarek, R. Ovalle-Robles, B. Wang, D. Hsu, A. A. Zakhidov, *Appl. Phys. Lett.* **2009**, *94*, 113506.

[201] K. Tohji, T. Goto, H. Takahashi, Y. Shinoda, N. Shimizu, B. Jeyadevan, I. Matsuoka, Y. Saito, A. Kasuya, T. Ohsuna, K. Hiraga, Y. Nishina, *Nature* **1996**, *383*, 679.

[202] N. Fukaya, D. Y. Kim, S. Kishimoto, S. Noda, Y. Ohno, *ACS Nano* **2014**, *8*, 3285.

[203] W. Xu, S. Wu, X. Li, M. Zou, L. Yang, Z. Zhang, J. Wei, S. Hu, Y. Li, A. Cao, *Adv. Energy Mater.* **2016**, *6*, 1600095.

[204] P.-X. Hou, B. Yu, Y. Su, C. Shi, L.-L. Zhang, C. Liu, S. Li, J.-H. Du, H.-M. Cheng, *J. Mater. Chem. A* **2014**, *2*, 1159.

[205] D. S. Hecht, L. Hu, G. Irvin, *Adv. Mater.* **2011**, *23*, 1482.

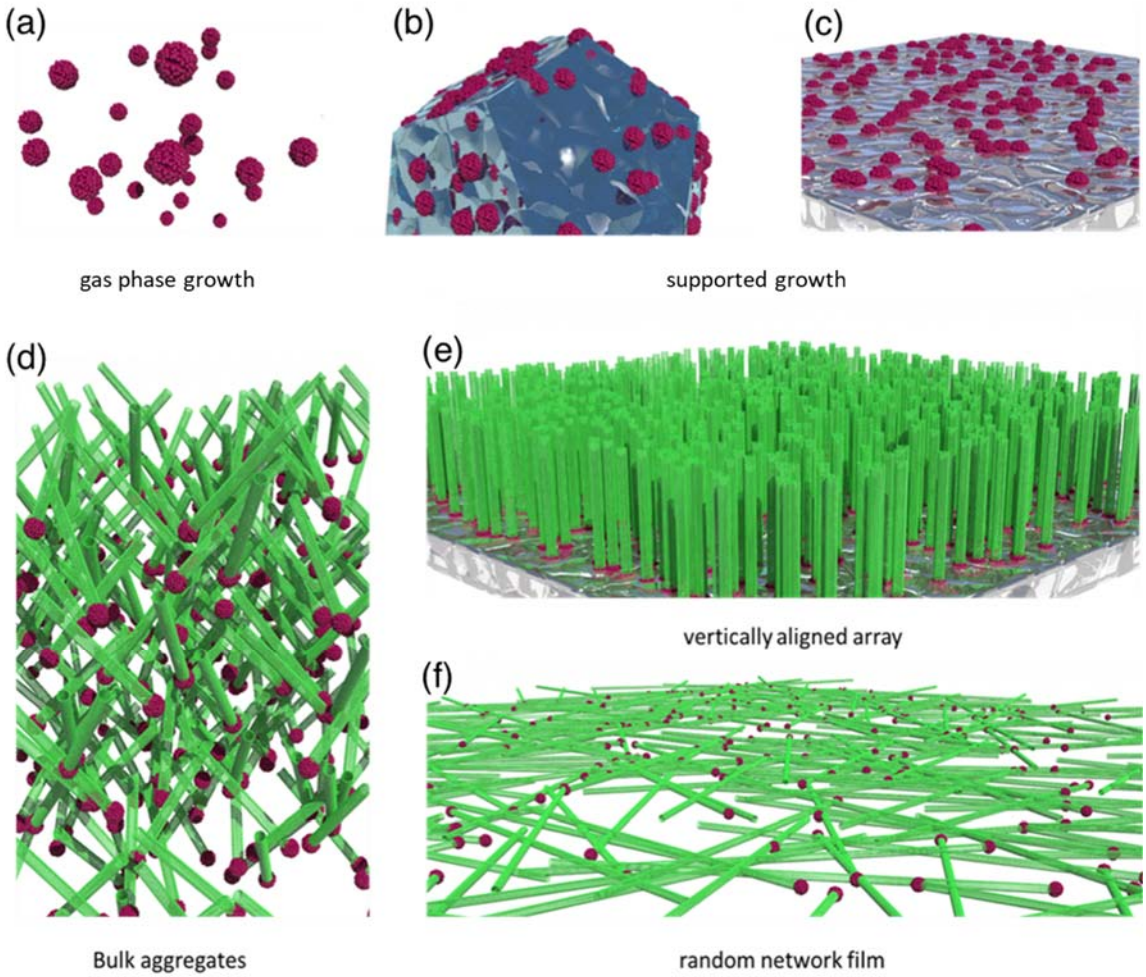

Figure 1. Schematics of the three major CVD synthesis protocols developed so far: (a) gas phase synthesis, (b) supported synthesis and (c) so called the on-substrate synthesis under a category of the supported synthesis. Different morphologies of SWNT product used in solar cell applications: (d) bulk aggregates, (e) vertically aligned array and (f) random network film.

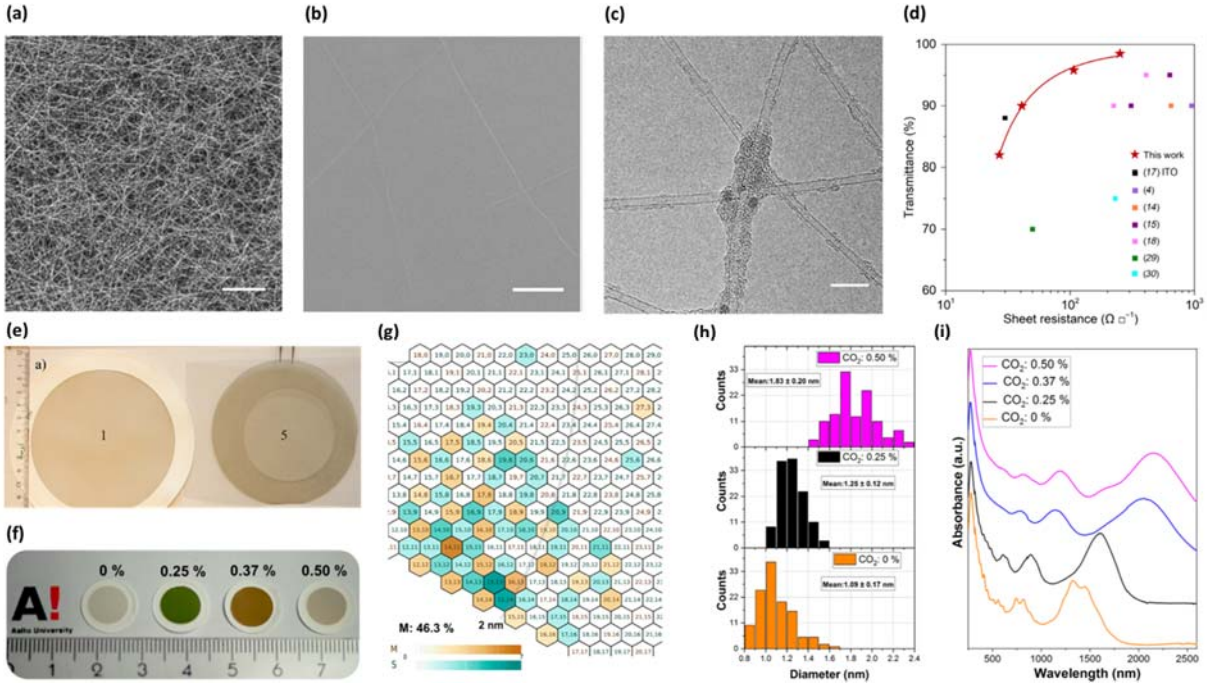

Figure 2. Large area SWNT films produced from floating and aerosol CVD: (a) SEM image (b) enlarged SEM image, (c) TEM image and (d) sheet resistance of highly isolated SWNT film produced from floating CVD (Reproduced with permission[30] copyright 2018, AAAS); (e) optical images of SWNT films produced from aerosol CVD, (f) optical images, (g) chirality distribution, (h) diameter distribution histogram, and (i) optical absorption spectra of pristine colored SWCNT films produced from aerosol CVD with addition of CO_2 (Reproduced with permission[40] copyright 2018, American Chemical Society).

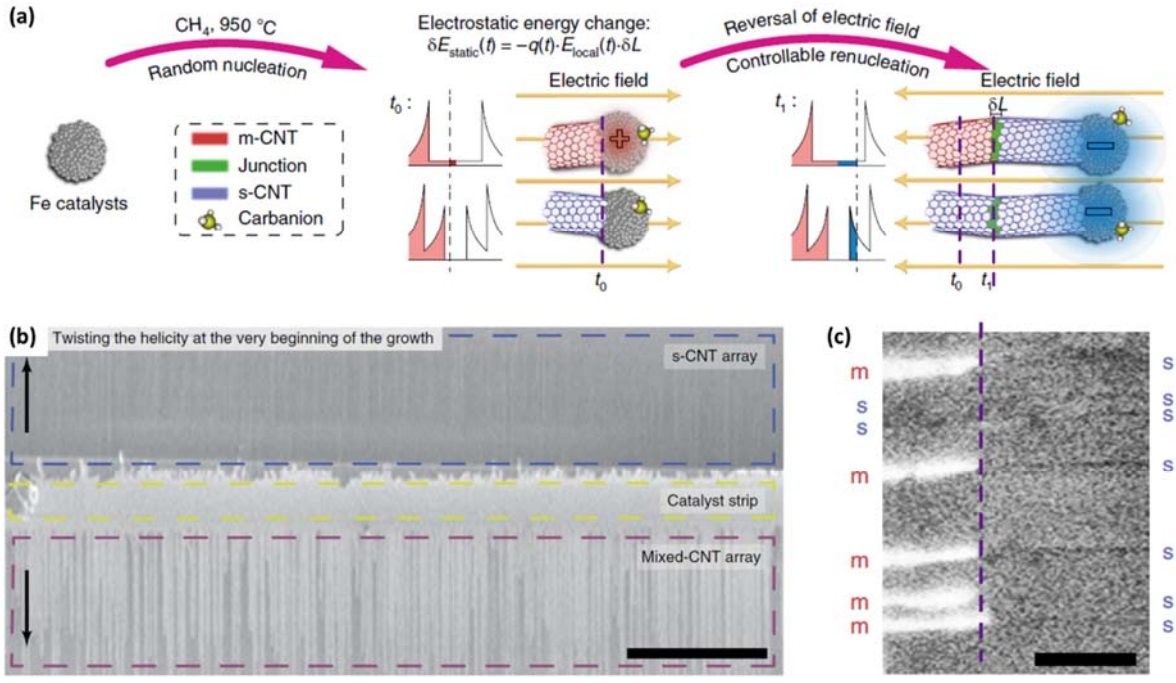

Figure 3. Highly pure semiconducting SWNT arrays grown by electro-twisting. (a) Schematic of reversing the electric field during CVD and its effect to SWNT chirality; (b) SEM image of

large area semiconducting SWNT arrays; (c) metal-semi junctions formed during in situ switching the electric field (Reproduced with permission[73] copyright 2018, Nature publishing group).

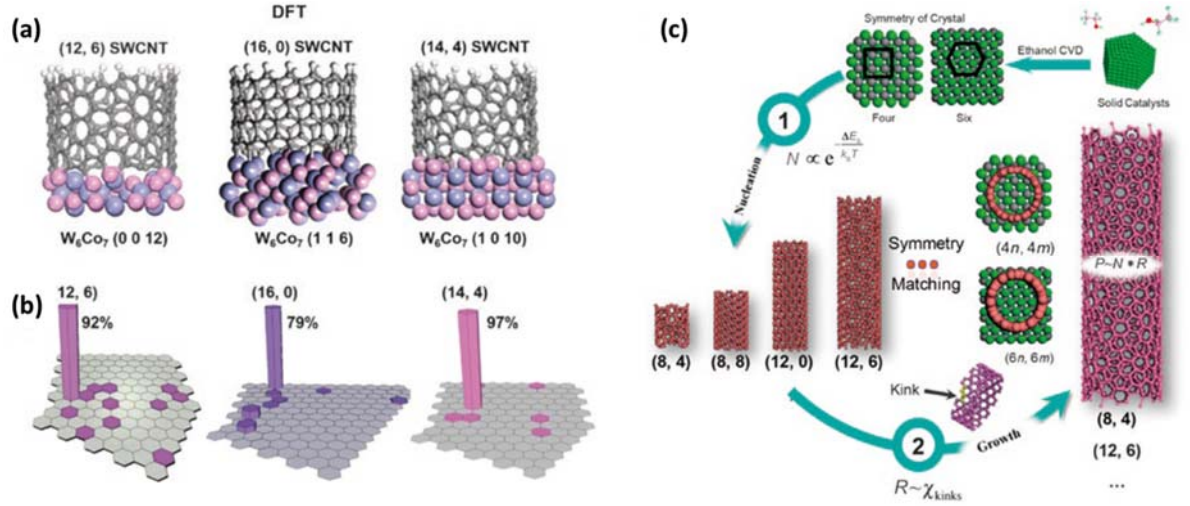

Figure 4. Chirality-specific growth of SWNT on solid catalyst: (a) DFT simulation of chirality selection on different facets of W_6Co_7, (b) population distribution obtained from experiments, and (c) a schematic to achieve growth of (2m,m) SWNTs by combining symmetry matching and dynamic control (Reproduced with permission[77] copyright 2018, Cambridge University Press).

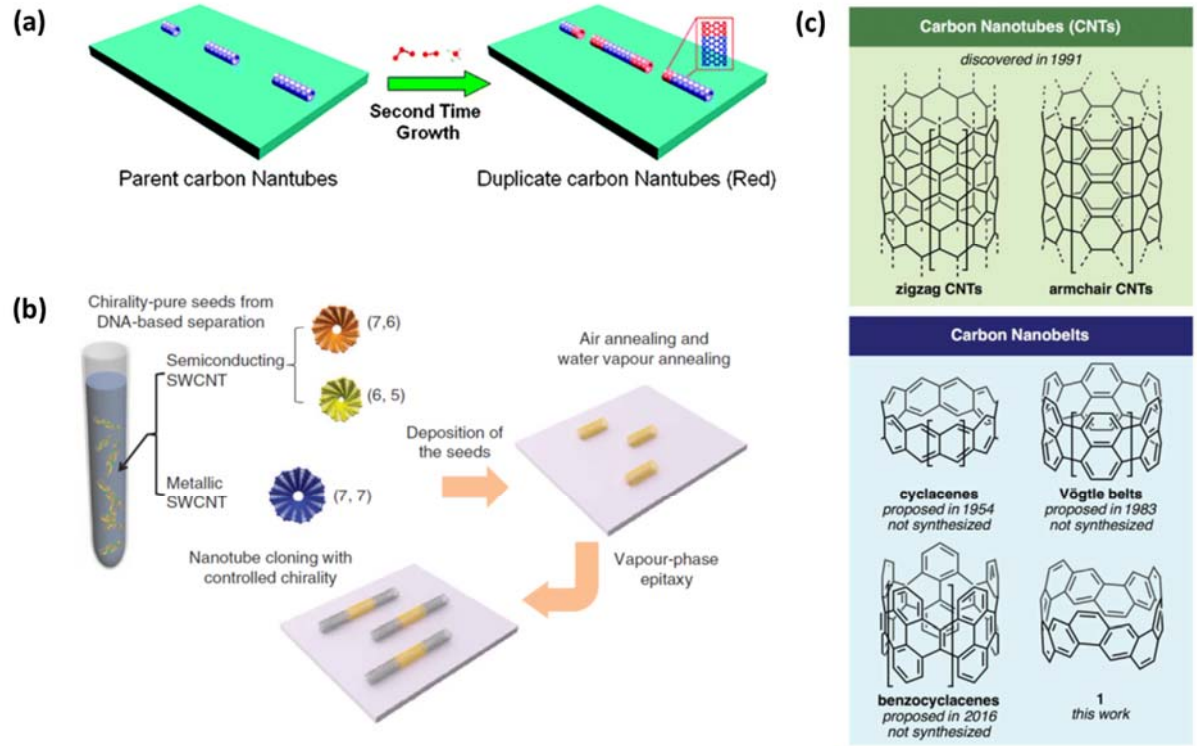

Figure 5. (a) Schematics of cloned growth of SWNTs from short segments (Reproduced with permission[88] copyright 2009, American Chemical Society). (b) Improved cloning growth from chirality pure nanotube seeds (Reproduced with permission[90] copyright 2012, Nature publishing group). (c) Successful synthesis of a carbon nanobelt that may be used for producing single-chirality SWNTs (Reproduced with permission[94] copyright 2017, AAAS).

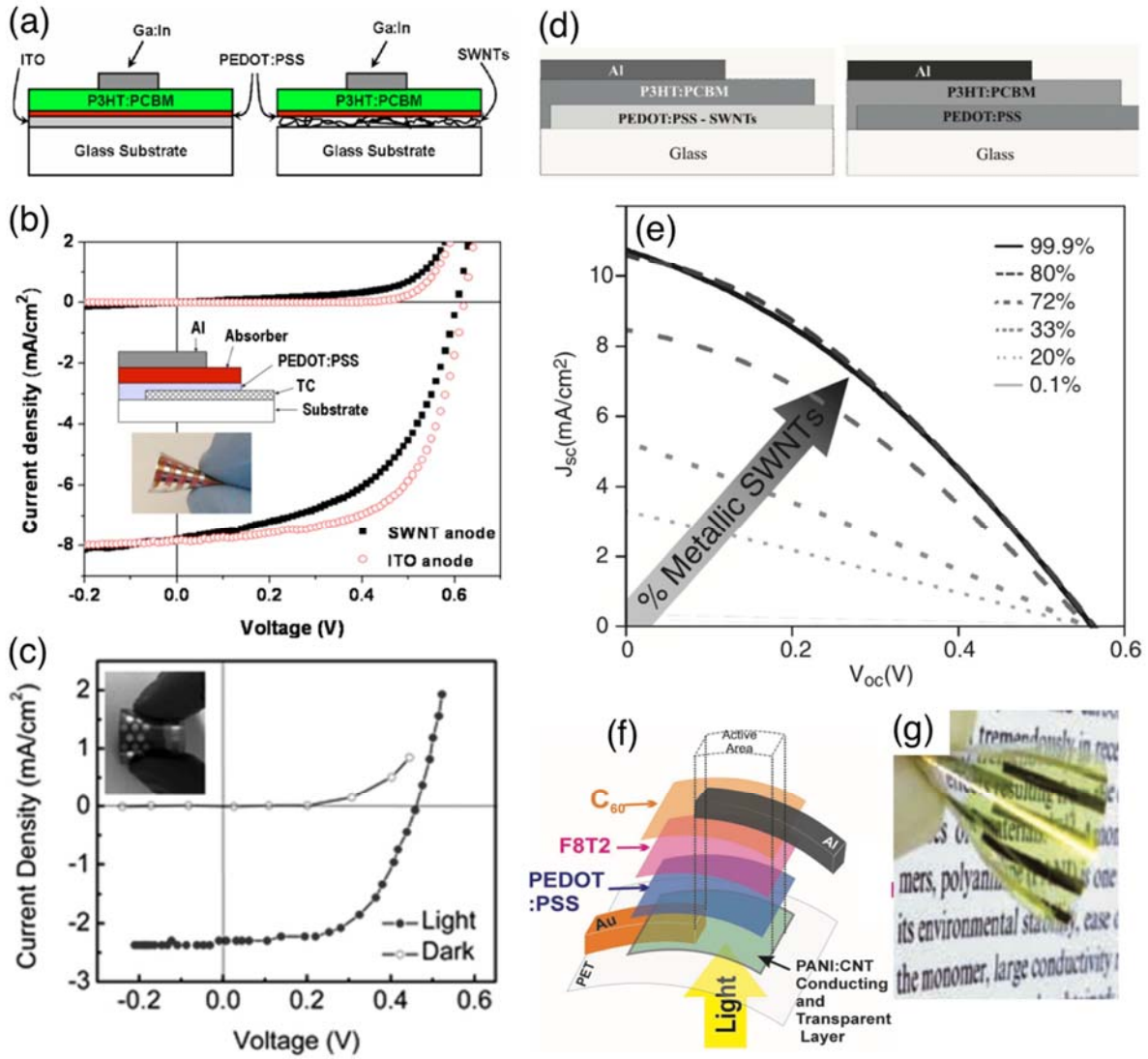

Figure 6. a) Schematic diagrams of the OSC devices with ITO as a transparent electrode (left) and SWNTs as the transparent electrode (right) (Table 2: Device A) (Reproduced with permission from *Appl. Phys. Lett.* **2005,** 87, DOI: 10.1063/1.2132065. Copyright 1998 American Chemical Society). b) *J–V* curves of the flexible OSCs using ITO (red circle) and SWNT (black circle) as a transparent conductor (TC) with its structure and a picture as insets (Table 2: Device B) (Reproduced with permission from *Appl. Phys. Lett.* **2006,** 88, DOI: 10.1063/1.2187945. Copyright 1998 American Chemical Society). c) *J–V* curve of the flexible OSCs from Table 2: Device C with its picture as an inset. (Reproduced from Ref. 121 with permission from the Royal Society of Chemistry) d) Schematics of the OSCs from Table 2: Device D (left) and Device E (right). e) *J–V* curves of SWNT-electrode-based OSC devices in which PCE is increasing with the metallic SWNT component (Table 2: Device H). f) Illustration of flexible OSCs in which CNT:PANI is used as the transparent conductor and g) its picture (Table 2: Device I).

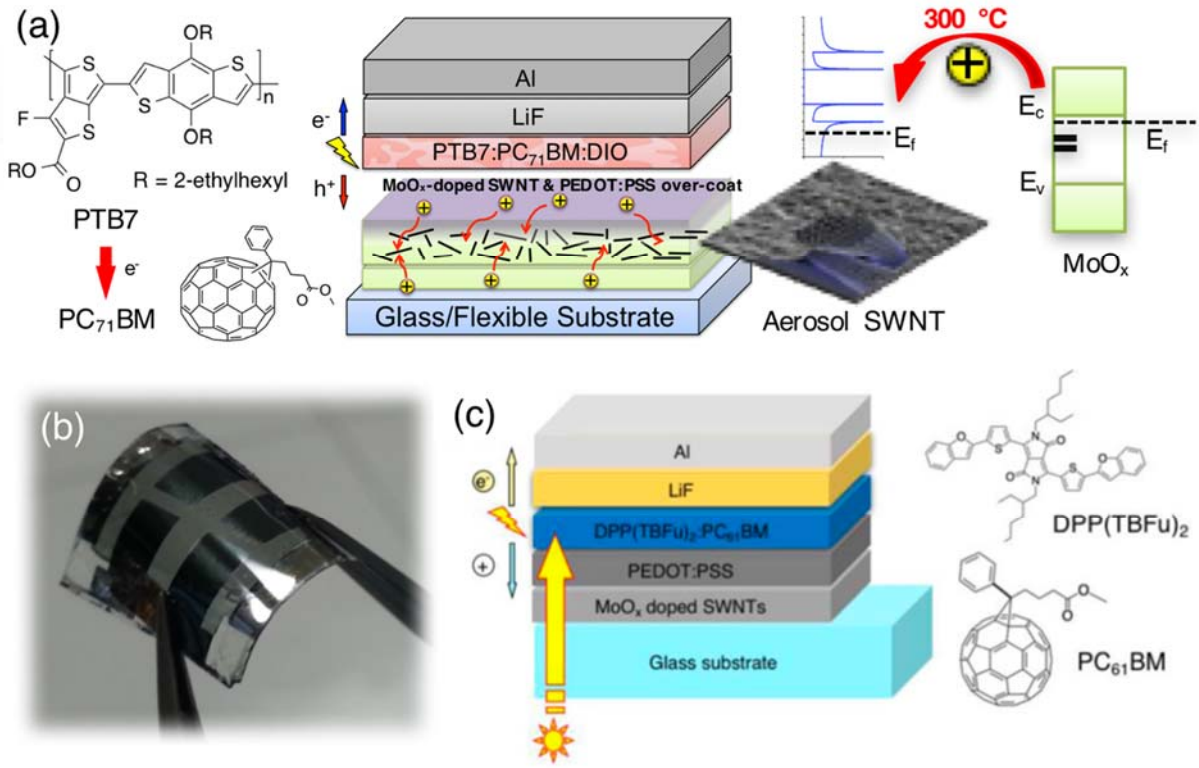

Figure 7. a) Schematic of the low-bandgap polymer OSC devices in which MoO_x doping on SWNT-electrode was used, showing molecular structures and a doping mechanism illustration. b) Structure of the SWNT-electrode-based small molecule OSCs from Table 2: Device J. c) A picture of the flexible OSC from Table 2: Device N.

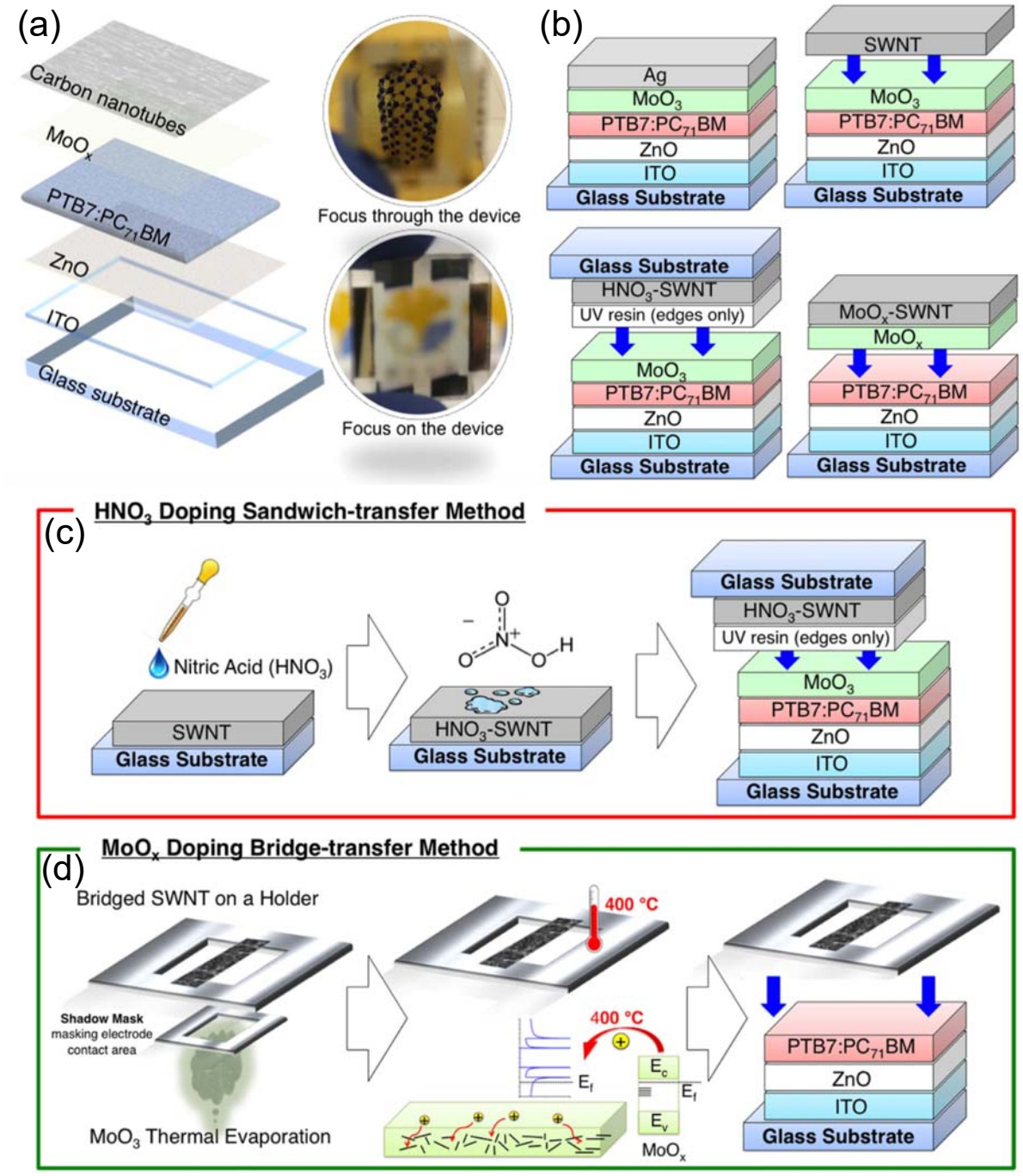

Figure 8. Structural illustration of the metal-free OSCs for window application from Table 2: Device P (left) and two pictures with different foci (right). b) four different OSCs fabricated in the same work,[136] including Device O and Device P from Table 2. Illustration of c) the HNO_3 doping sandwich-transfer method, and d) the MoO_x doping bridge-transfer method (Reproduced from Ref. 136 with permission from Nature Publishing Group).

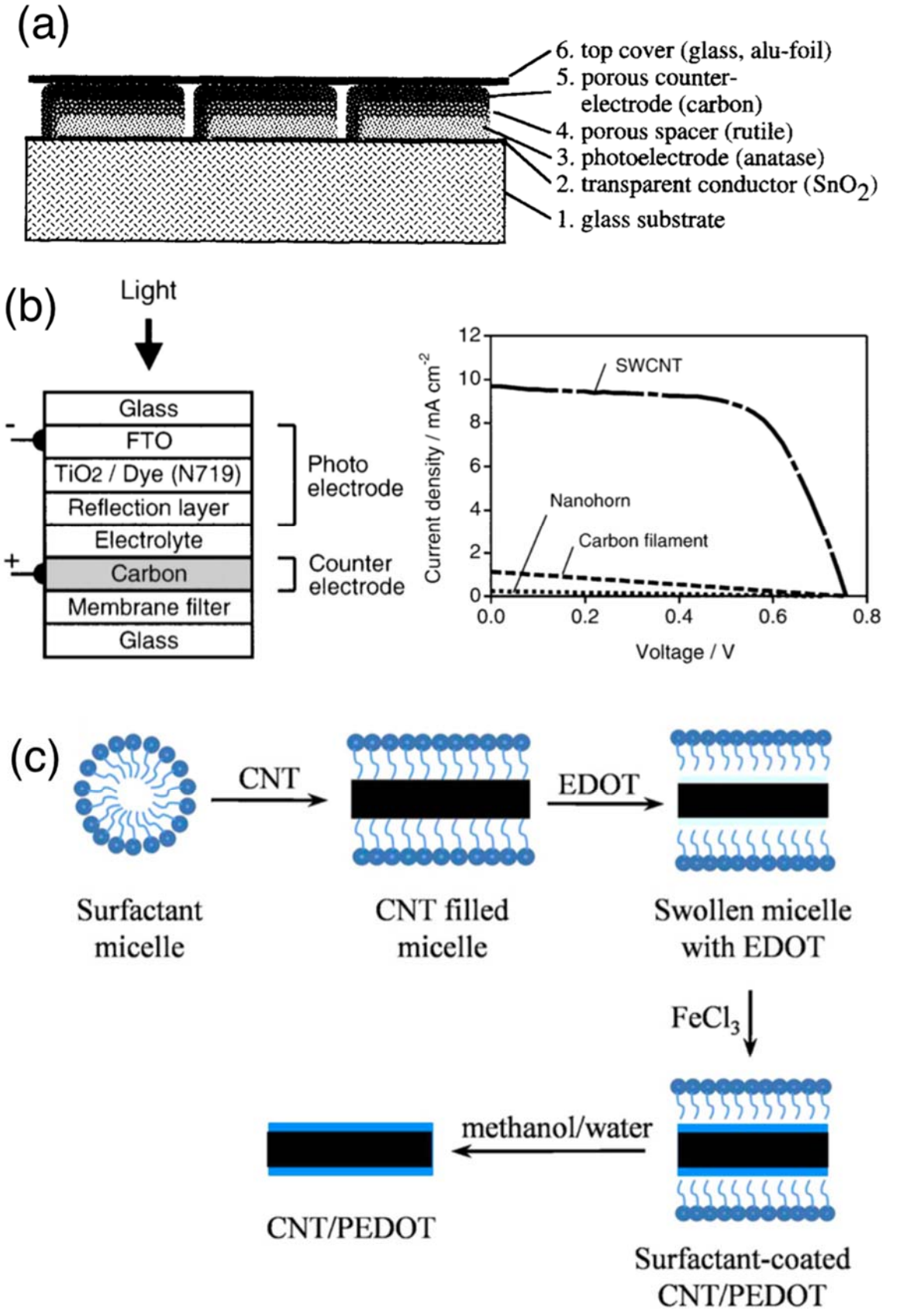

Figure 9. a) Schematic cross section of the monolithic series connected dye sensitized photovoltaic module (Copyright © 1996 Published by Elsevier B.V.). b) Schematic diagram of DSSC with carbon film as a counter electrode (left) and *J–V* curves of the device using various carbon electrodes (right). c) Schematic illustration for the synthesis of CNT/PEDOT core/shell nanostructures (Copyright © 1996 Published by Elsevier B.V.).

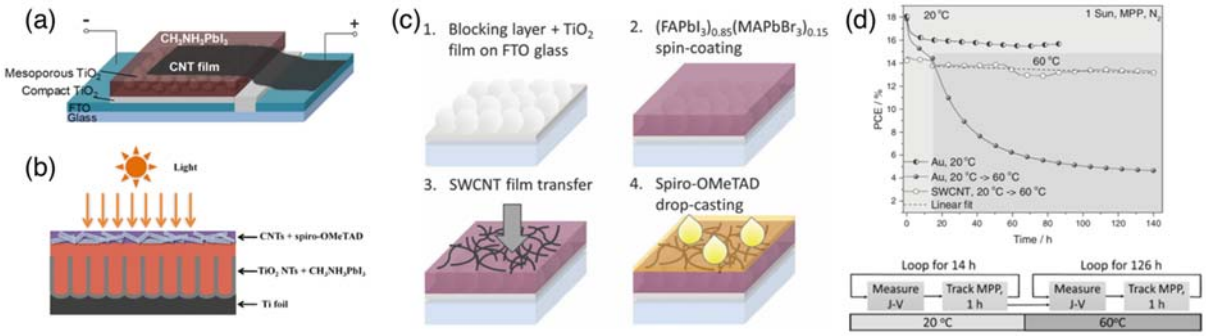

Figure 10. a) Schematic diagram of the first SWNT-electrode application in PSCs (Table 3: Device B). b) Schematic diagram Ti foil-based PSCs in which CNTs have been used as the top electrode (Table 3: Device D) (Copyright © 1996 Published by Elsevier B.V.). c) Sequential diagrams explaining how SWNT top electrode PSCs are fabricated (Table 3: Device F) (Reproduced from Ref. 157 with permission from the Royal Society of Chemistry). D) Results of maximum power point tracking curves of Au- and SWNT-based PSCs at elevated temperatures (above), and illustration of the measurement conditions in which temperature of the devices was changed from 20 ºC to 60 ºC after 14 h (blow).

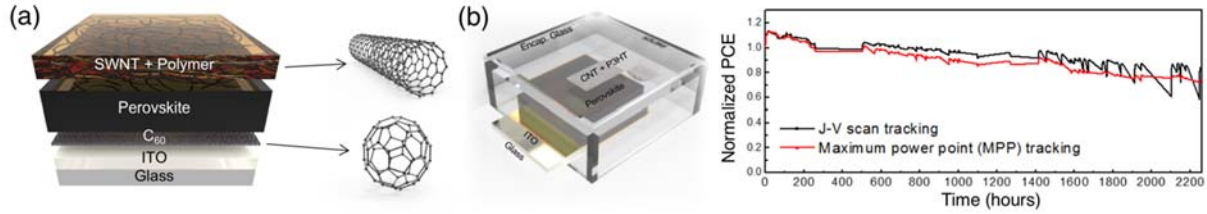

Figure 11. a) Illustration of the carbon-sandwiched PSCs (Table 3: Device I and J). b) 3D image of an encapsulated carbon-sandwiched PSC with P3HT as the hole-transporting layer (left) and its stability data (Reproduced from Ref. 167 with permission from the Royal Society of Chemistry).

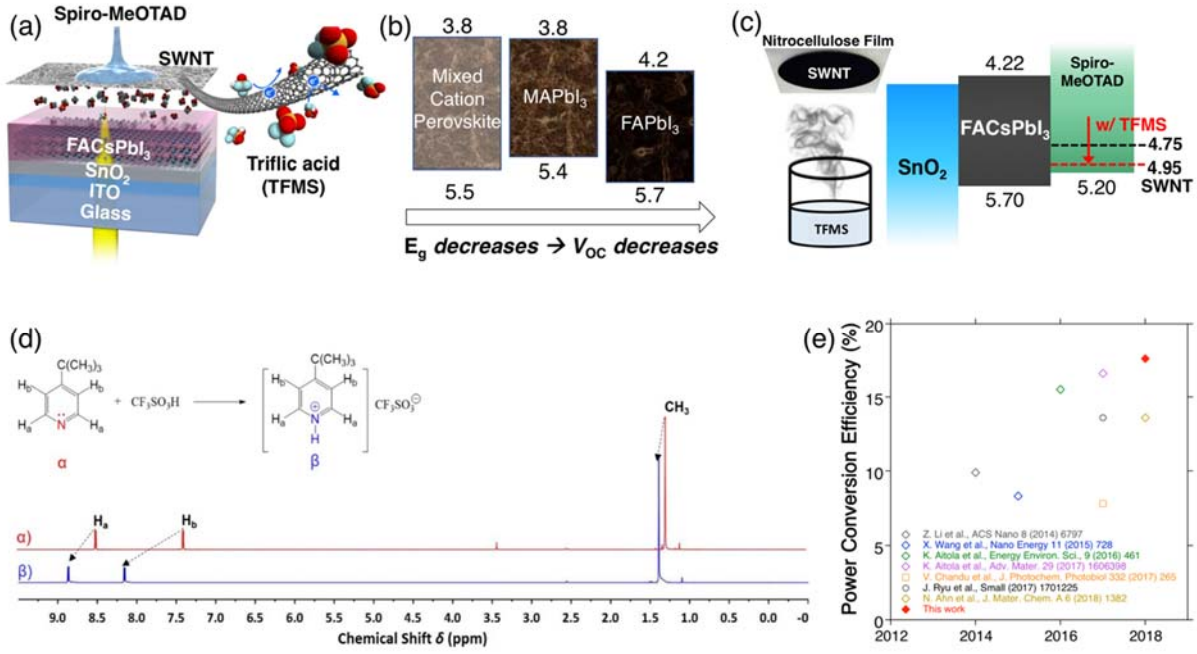

Figure 12. a) Illustration of $FACsPbI_3$-based PSCs with TFMS-doped SWNT as the top electrode (Table 3: Device K). b) Energy diagrams of three different perovskite materials. c) TFMS vapor doping illustration and the energy level change. d) ^1H NMR spectra were recorded in DMSO-d_6 solution at 500 MHz. α) ^1H NMR of 4-*tert*-butylpyridine; β) ^1H NMR of 4-*tert*-butylpyridine with addition of 10 wt% of TFMS. e) PCE chart showing the the SWNT top electrode-based PSCs reported thus far.

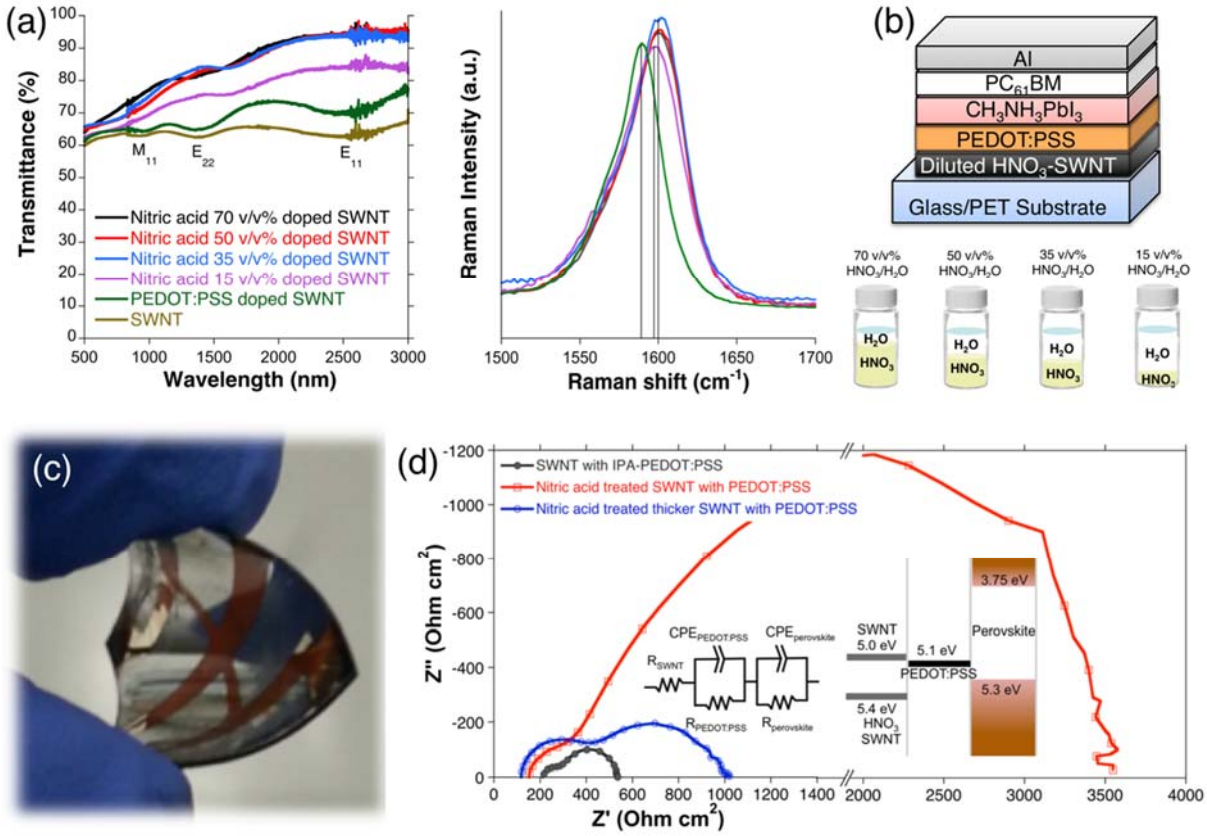

Figure 13. a) Vis-near IR spectra (left) and Raman spectra (right) of the SWNT films treated by different HNO_3(aq) concentrations. b) Schematic diagram of a SWNT-electrode-based

PSC with different HNO_3(aq) concentrations as illustrations. c) A picture of a flexible SWNT-electrode-based PSC. d) Impedance spectra of different SWNT-electrodes in contact with the perovskite material, and a corresponding electric circuit and an energy diagram as insets.

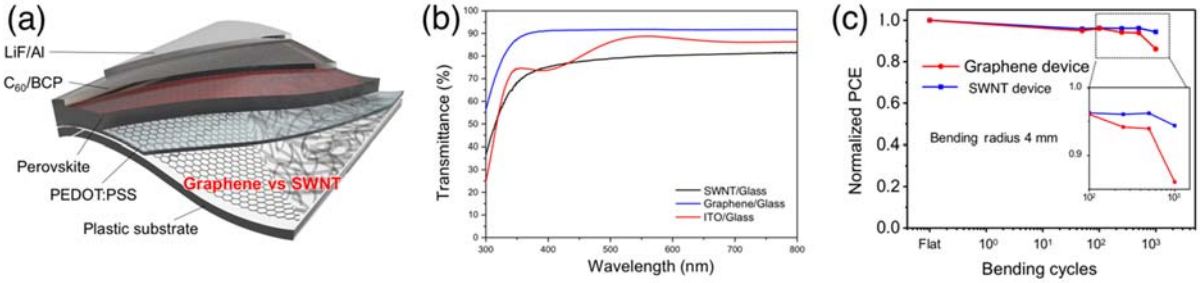

Figure 14. a) 3D rendering image of a SWNT and graphene transparent electrode-based PSC. b) UV-vis transmittance spectra of SWNT (black), graphene (blue), and ITO (red) on glass substrates. c) AFM (left) and cross-sectional SEM (right) images of graphene (above) and SWNT (below). c) Cyclic flexural test of graphene-based PSCs (red) and SWNT-based PSCs (blue).

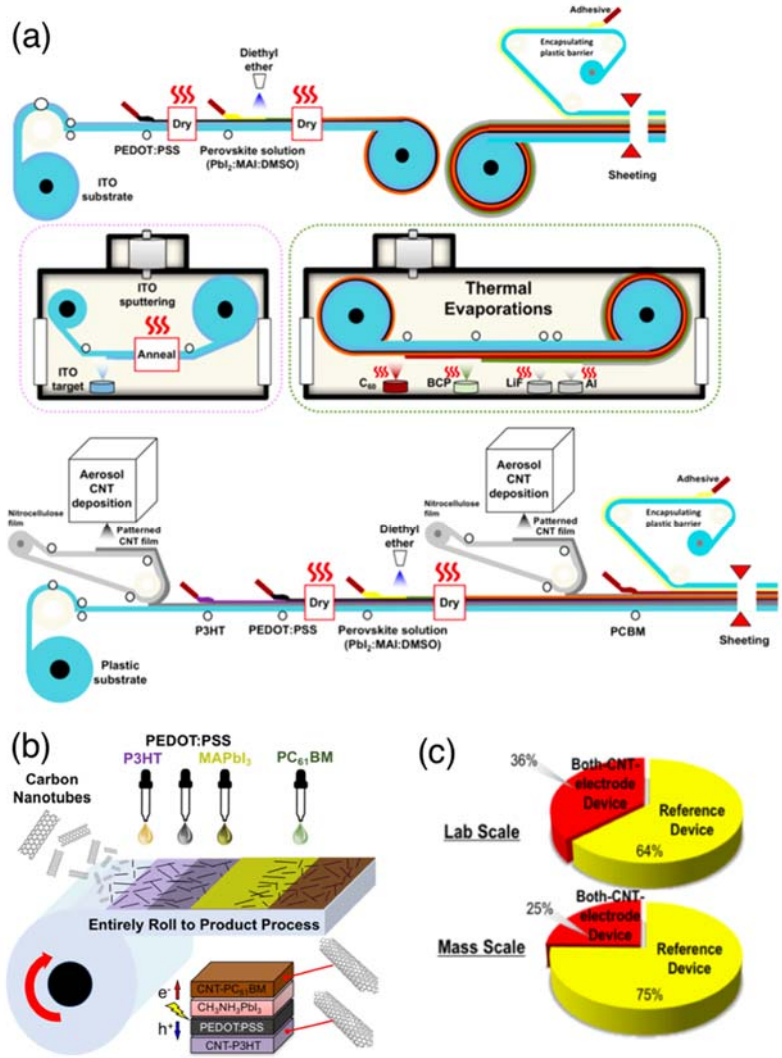

Figure 15. a) Process illustration of conventional PSC fabrication (above) and non-stop continuous both-SWNT-electrode PSC fabrication. b) Simplified illustration of the entirely solution-processable OSCs. c) Cost analytsis pie charts of both-CNT-electrode PSCs (red) and conventional PSCs (yellow) for the lab scale (above) and the mass scale (below).

Table 1. List of SWNT syntheses discussed in Section 2. Growth type, process name, carbon source, and product characteristics are summarized.

Growth	Process	Name	Carbon Source	Product Form	Diameter (nm)	Length (μm)	Chirality
Gas-Phase Growth	A	HiPco	CO	Powder	*ca.* 1	0.1-1	Broad
	B	CoMoCAT	CO	Powder	*ca.* 0.8	2-5	(6,5)
	C	ACCVD	Ethanol	Powder	*ca.* 1	2-5	(6,5)
	D	Floating CVD	Benzene	Fibers	*ca.* 2	10-50	N/A
	E	eDIPS	Toluene/Ethene	Powder	1.2-1.8	2-5	N/A
	F	Aerosol	CO	Film	1.3-2	1-5	Broad
	G	Zeolite	CO	Powder	*1-2*	2-5	(7,5) (7,6) (8,4)
Supported Growth (On-Substrate Growth)	H	ACCVD2	Ethanol	VA-forest	0.8-2	<100	Broad
	I	Super Growth	Ethene		1.5-3	<1000	N/A
	J	Flow-Guided Growth	CO/Methane	HA-CNT	1-4	<50000	N/A
	K	Crystal-Guided Growth	Methane/Ethanol				Broad

Table 2. List of reported OSCs in which electrodes have been replaced by SWNT (or CNT) electrodes.

Ref.	Device	Structure	J_{SC} (mA cm^{-2})	V_{OC} (V)	FF	PCE (%)
[118]	A	glass/SWNT/PEDOT:PSS/P3HT:PCBM/Ga-In	6.65	0.50	0.3	0.99
[120]	B	PET/SWNT/PEDOT:PSS/P3HT:PCBM/Al	7.8	0.61	0.52	2.5
[121]	C	PET/SWNT/ZnO nanowire/P3HT/Au	-	-	-	0.6
[122]	D	glass/SWNT/PEDOT:PSS/P3HT:PCBM/Al	5.6	0.58	0.4	1.3
	E	glass/PEDOT:PSS/P3HT:PCBM/Al	1	0.55	0.35	0.2
[124]	F	glass/SWNT(DCE)/P3HT:PCBM/LiF/Al	9.9	0.55	0.43	2.3
	G	glass/SWNT(H_2O:SDS)/P3HT:PCBM/LiF/Al	7.3	0.59	0.46	2.2
[125]	H	glass/SWNT(metallic)/P3HT:PCBM/LiF/Al	10.7	0.56	0.34	2.0
[127]	I	PET/CNT:PANI/PEDOT:PSS/F8T2/C_{60}/Al	6.9	0.73	0.45	2.3
[131]	J	glass/SWNT/MoO_3/PEDOT:PSS/PTB7:PC_{71}BM/LiF/Al	12.7	0.70	0.58	5.3
	K	glass/SWNT/MoO_x/PEDOT:PSS/PTB7:PC_{71}BM/LiF/Al	13.7	0.72	0.61	6.0
	L	PI/SWNT/MoO_x/PEDOT:PSS/PTB7:PC_{71}BM/LiF/Al	11.3	0.69	0.44	3.4
	M	PET/SWNT/MoO_3/PEDOT:PSS/PTB7:PC_{71}BM/LiF/Al	12.7	0.70	0.45	3.9
[103]	N	glass/SWNT/MoO_x/PEDOT:PSS/DPP(TBFu)2:PCBM/LiF/Al	3.2	0.8	0.40	1.9

[136]	O	glass/ZnO/PTB7:$PC_{71}BM$/MoO_3/HNO_3-SWNT/glass	9.0	0.70	0.65	4.1
	P	glass/ZnO/PTB7:$PC_{71}BM$/HNO_x-SWNT	8.2	0.68	0.60	3.4

Table 3. List of reported PSCs in which electrodes have been replaced by SWNT (or CNT) electrodes.

Ref.	Device	Structure	J_{SC} (mA cm^{-2})	V_{OC} (V)	FF	PCE (%)
[155]	A	glass/FTO/c-TiO_2[a]/m-TiO_2[b]/$MAPbI_3$/SWNT	14.7	0.83	0.49	6.02
	B	glass/FTO/c-TiO_2/m-TiO_2/$MAPbI_3$/spiro-MeOTAD/SWNT	18.1	1.00	0.55	9.90
[156]	C	Ti foil/nt-TiO_2[c]/$MAPbI_3$/spiro-MeOTAD/SWNT+DWNT	12.2	0.77	0.60	4.83
	D	Ti foil($TiCl_4$-treated)/nt-TiO_2/$MAPbI_3$/spiro-MeOTAD/SWNT+DWNT	12.6	0.97	0.60	7.38
[157]	E	glass/FTO/c-TiO_2/m-TiO_2/$(FAPbI_3)_{0.85}(MAPbBr_3)_{0.15}$/SWNT	20.3	0.97	0.46	11.0
	F	glass/FTO/c-TiO_2/m-TiO_2/$(FAPbI_3)_{0.85}(MAPbBr_3)_{0.15}$/spiro-MeOTAD/SWNT	20.3	1.1	0.61	15.5
[159]	G	glass/FTO/c-TiO_2/m-TiO_2/$Cs_5(MA_{0.17}FA_{0.83})_{95}Pb(I_{0.83}Br_{0.17})_3$/spiro-MeOTAD/SWNT	21.0	1.12	0.71	16.6
[161]	H	glass/FTO/c-TiO_2/$MAPbI_3$/CNT	18.5	0.70	0.6	10.7
[162]	F	glass/FTO/c-TiO_2/m-TiO_2/$Cs_5(MA_{0.17}FA_{0.83})_{95}Pb(I_{0.83}Br_{0.17})_3$/CNT	19.0	1.00	0.71	13.6
[167]	G	glass/ITO/C_{60}/$MAPbI_3$/SWNT	21.8	0.93	0.65	13.2
	H	glass/ITO/C_{60}/$MAPbI_3$/spiro-MeOTAD/SWNT	23.8	1.08	0.66	17.0
	I	glass/ITO/C_{60}/$MAPbI_3$/PTAA/SWNT	23.0	0.98	0.68	15.3
	J	glass/ITO/C_{60}/$MAPbI_3$/P3HT/SWNT	21.7	0.94	0.67	13.6
[169]	K	glass/ITO/SnO_2/$FACsPbI_3$/spiro-MeOTAD/TFMS-SWNT	24.2	1.01	0.72	17.6
[177]	L	glass/HNO_3-SWNT/PEDOT:PSS/$MAPbI_3$/$PC_{61}BM$/Al	14.9	0.79	0.54	6.32
	M	glass/SWNT/PEDOT:PSS/$MAPbI_3$/$PC_{61}BM$/Al	11.8	0.61	0.38	2.71
	N	glass/SWNT/PEDOT:PSS/$MAPbI_3$/$PC_{61}BM$/Al	11.1	0.77	0.50	4.27
	O	PET/HNO_3-SWNT/PEDOT:PSS/$MAPbI_3$/$PC_{61}BM$/Al	11.8	0.71	0.56	5.38
[181]	P	glass/graphene/MoO_3/PEDOT:PSS/$MAPbI_3$/C_{60}/BCP/Ag	21.2	0.96	0.70	14.2
	Q	glass/SWNT/MoO_3/PEDOT:PSS/$MAPbI_3$/C_{60}/BCP/Ag	17.5	0.96	0.76	12.8
[188]	R	glass/HNO_3-SWNT/PEDOT:PSS/$MAPbI_3$/$PC_{61}BM$/Al	18.3	0.81	0.66	9.8
	S	glass/ITO/PEDOT:PSS/$MAPbI_3$/$PC_{61}BM$/SWNT	18.1	0.79	0.73	10.5
	T	glass/SWNT/P3HT/PEDOT:PSS/$MAPbI_3$/$PC_{61}BM$/SWNT	15.9	0.80	0.57	7.32
[196]	U	PET/graphene/TiO_2/PCBM/$MAPbI_3$/spiro-MeOTAD/CNT	20.3	0.89	0.65	11.9

[a] c-TiO_2: compact-TiO_2; [b] mp-TiO2: mesoporous-TiO_2; c) nt-TiO_2: nanotube array-TiO_2

Il Jeon read Chemistry for Bachelors and Masters degrees at the University of Oxford, UK in 2008. Upon graduation, he worked as the youngest senior researcher in LG Display Co. Ltd., South Korea for 5 years, developing optical films, OLED, and quantum displays. In 2016, he received a PhD degree in Chemistry with honours at the University of Tokyo, Japan. Having worked as a JSPS postdoctoral fellow and an assistant professor, he is now a lecturer (senior assistant professor) in the same university. His research focuses on the development of carbon allotropes and their optoelectronic applications.

Shigeo Maruyama is a distinguished professor at the University of Tokyo. He is also serving as a cross-appointment fellow at Department of Energy and Environment at National Institute of Advanced Industrial Science and Technology (AIST). He received PhD at the University of Tokyo in 1988, and worked at the University of Tokyo. He has been serving as the president of The Fullerenes, Nanotubes and Graphene Research Society (FNTG) since 2011. His research interest is growth, characterization, and solar cell application of low-dimensional materials such as carbon nanotubes, graphene and transition metal dichalcogenides (TMDC).

Single-walled carbon nanotube electrodes in organic solar cells and perovskite solar cells are reviewed in synthesis and applications point of views. The emerging thin-film solar cells have the potential to become next-generation flexible and portable energy devices. Replacement of conventional electrodes by single-walled carbon nanotubes is crucial in achieving such devices. This review summarizes the progress of this.

Keyword: single-walled carbon nanotubes, carbon electrodes, photovoltaics, organic solar cells, perovskite solar cells

I. Jeon, R. Xiang, A. Shawky, Y. Matsuo, S. Maruyama*

Single-Walled Carbon Nanotubes in Emerging Solar Cells: Synthesis and Electrode Applications